



HAL
open science

The thermo-mechanical behaviour of the Callovo-Oxfordian claystone

Hamza Menaceur, Pierre Delage, Anh Minh A.M. Tang, Nathalie Conil

► **To cite this version:**

Hamza Menaceur, Pierre Delage, Anh Minh A.M. Tang, Nathalie Conil. The thermo-mechanical behaviour of the Callovo-Oxfordian claystone. *International Journal of Rock Mechanics and Mining Science & Geomechanics Abstracts*, 2015, 78, pp.190-303. 10.1016/j.ijrmms.2015.07.002 . hal-02104941

HAL Id: hal-02104941

<https://enpc.hal.science/hal-02104941>

Submitted on 19 Apr 2019

HAL is a multi-disciplinary open access archive for the deposit and dissemination of scientific research documents, whether they are published or not. The documents may come from teaching and research institutions in France or abroad, or from public or private research centers.

L'archive ouverte pluridisciplinaire **HAL**, est destinée au dépôt et à la diffusion de documents scientifiques de niveau recherche, publiés ou non, émanant des établissements d'enseignement et de recherche français ou étrangers, des laboratoires publics ou privés.

1 **Abstract:**

2 The Callovo-Oxfordian (COx) claystone is considered as a potential host rock in the
3 French concept of high level radioactive waste disposal at great depth. To better
4 understand and to complement existing published data on the thermo-hydro-mechanical
5 behaviour of the COx claystone, an experimental program was carried out by using a
6 hollow cylinder triaxial device specially developed for low permeability materials.
7 Special care was devoted to the saturation of the specimens that was made under stress
8 conditions close to in-situ, and to conditions ensuring full drainage thanks to a reduced
9 drainage length and low shear rate. Tests were carried out under in-situ, half to in-situ
10 and twice the Terzaghi mean effective in-situ stress at 25°C and 80°C to investigate the
11 effects in the close field of the temperature elevation due to the exothermic nature of
12 the waste. Some radial permeability tests were conducted at various temperatures. The
13 data obtained showed that there is little effect of temperature on the elastic parameters
14 determined, whereas a tendency to a decrease in shear strength was noted, compatible
15 with the few published data. Temperature also appeared to have little effect on the
16 intrinsic permeability, with higher flows mainly due to the decrease in water viscosity.

17
18
19
20
21
22
23
24
25

1 **1. Introduction**

2
3 In many countries (including Belgium, France and Switzerland), deep argillaceous
4 formations are considered as potential host rock for the disposal of high activity
5 radioactive waste at great depth. Because of low permeability, good self sealing
6 properties and ability to retain radionuclides, the Callovo-Oxfordian (COx) claystone
7 has been selected in France as potential host rock by Andra, the French agency for the
8 management of radioactive waste. Andra developed an Underground Research
9 Laboratory [1] in the COx layer at a depth of 490 m near the village of Bure (East of
10 France) to perform in-situ investigations devoted to various aspects of radioactive waste
11 disposal, including the thermo-hydro-mechanical response of the host rock in the close
12 field, in configurations close to that prevailing during the operational phase of the waste
13 disposal [1].

14 In the French concept, the canisters containing the radioactive waste are to be
15 placed in disposal cells that consist in horizontal cased microtunnels of 70 cm in
16 diameter and at least 80 m in length. Due to the exothermic nature of radioactive
17 wastes, the rock in the close field and the excavation damaged zone (EDZ) around
18 disposal cells and galleries will be submitted to a temperature elevation. A maximum
19 temperature of 90°C at the cells wall is considered in the French concept, a condition
20 that has obvious economic consequences in terms of both the density of the network of
21 gallery and disposal cells and the number of canisters that can be placed along a given
22 length of excavated disposal cell.

23 Various investigations have been carried out on the thermal behaviour of clays but
24 that of claystones is much less documented. In clays, the importance of the
25 overconsolidation ratio has clearly been emphasized, with significant effects in volume
26 change and shear strength response [1, 2, 3, 4, 5, 6].

1 Various investigations have been carried out about the hydro-mechanical
2 behaviour of the COx claystone based on triaxial tests [7, 8, 9, 10, 11]. Actually,
3 published data on the shear strength properties of the COx claystone appear to be
4 somewhat dispersed partly due to the natural variability of the properties of the
5 claystone. The mineralogical composition of the COx claystone changes with depth, in
6 particular in terms of clay and calcite content. The depth of 490 m at which the Bure
7 URL has been excavated corresponds to a maximum clay content of around 50%,
8 selected to ensure the best isolating properties in terms of low permeability, self-sealing
9 and radionuclides retaining ability.

10 Another possible reason of the observed dispersion of the published mechanical
11 characteristics of the COx is related to the various testing methodologies adopted. A
12 first important parameter is the specimen size that obviously controls the easiness and
13 the period of time necessary to fully saturate specimens. Claystone specimens can be
14 significantly desaturated due to the consecutive effects of coring, core isolation from
15 evaporation, core transportation and storage and, finally, machining in the laboratory.
16 Claystones are very sensitive to changes in water content and triaxial tests carried out at
17 various degrees of saturation evidenced a significant increase of the mechanical
18 strength with lower degree of saturation [8, 9, 12, 13, 14].

19 Another parameter largely dependent on the specimen size is the quality of the
20 drainage ensured during triaxial testing. Due to the very low permeability of claystones
21 (around 10^{-20} m² for the COx claystone), fully drained tests that are necessary for a
22 sound determination of their intrinsic mechanical characteristics are difficult to achieve
23 [15]. Good drainage can be ensured either by adopting slow enough shearing rate or by
24 adopting testing devices with small drainage length. This can be made either by testing

1 small specimens or by adopting specimen shapes with reduced drainage length [15, 16,
2 11]. These aspects will be commented in more details later.

3 In this paper, fully saturated and fully drained triaxial thermal tests were carried
4 out on COx specimens by using a hollow cylinder thermal triaxial device with short
5 drainage length specially developed for low permeability geomaterials [16]. This
6 thermal device has already successfully been used to test the Boom clay from Belgium
7 [17], the Opalinus clay from Switzerland [18] and the COx claystone from France [19].
8 The experimental program carried out here was aimed at further investigate the effects
9 of temperature on the shear strength response of the COx claystone by comparing tests
10 carried out at 80°C with tests run at 25°C, following the work of Mohajerani et al. [19]
11 on thermal volume changes. Triaxial tests were complemented by constant head radial
12 permeability tests run at both temperatures to investigate the effects of temperature on
13 permeability.

14 **2. The Callovo-Oxfordian claystone**

15

16 *2.1. Mineralogical composition*

17 The COx claystone is a sedimentary rock deposited 155 millions years ago on top of a
18 layer of Dogger limestone that was afterwards covered by an Oxfordian limestone
19 layer. The thickness of the COx layer is about equal to 150 m. The COx claystone is
20 composed of a clay matrix containing some grains quartz and calcite with a
21 mineralogical composition depending on depth with significant changes in carbonate
22 and clay contents. At the depth of the Bure URL (490 m), the average mineralogical
23 composition of COx claystone is as follows [20]: 45-50% clay fraction composed of
24 10-24% interstratified illite/smectite layers, 17-21% illite, 3-5% kaolinite, 2-3%
25 chlorite. The claystone also contains 28% carbonate, 23% quartz and 4% other minerals
26 (feldspars, pyrite, dolomite, siderite and phosphate minerals). The total porosity varies

1 in the COx layer between 14% in carbonated levels and 19.5% in the more argillaceous
2 levels [21].

3 The characteristics of the specimens tested are presented in Table 1. Specimens
4 come from various cores named EST45414 (specimen S1, depth 498 m), EST30734
5 (S2, depth 612 m) and EST285nn (S3-S4, depth 479 m) and EST45407 (S5, depth
6 499m). These cores have been extracted at distinct locations. They were selected
7 because they are located approximately at the same level in the claystone layer.
8 Specimen S1 and S5 have a porosity between 13 and 13.5% and a water content around
9 2.2% corresponding to degrees of saturation between 38 and 39%. A suction of
10 109 MPa was measured in specimen S1 by using a WP4 dew-point tensiometer.
11 Specimens S2, S3 and S4 have larger porosity between 16.5 and 17.8%, higher water
12 content of around 6% corresponding to degrees of saturation between 80 and 85%. The
13 suctions of specimens S2 and S4 are equal to 31 and 34 MPa, respectively.

14 *2.2. Shear strength and thermal effects in the COx claystone*

15 Published data about the shear properties of the COx claystone determined by running
16 triaxial tests are variable. This is due to the natural variability observed in the COx
17 claystone layer. The specimens tested do not necessarily come from the same borehole
18 location or from the same depth whereas the mineralogical composition of the claystone
19 is dependent upon the depth at which the specimen has been cored. For instance,
20 specimens with higher calcite content and smaller clay content extracted from layers
21 deeper than that of the Bure URL (that is located at the level of maximum clay content)
22 are stiffer and stronger, as recently confirmed in terms of Young modulus by means of
23 micro-indentation and mini compression tests (UCS) run by Hu et al. [22] on COx
24 unsaturated specimens extracted from depths of 490, 503 and 522 m. By testing COx
25 specimens from various depths, Chiarelli [7] showed that the Young modulus increased

1 with larger calcite content (between 6 and 15 GPa for calcite content between 20 and
2 52%) and decreased with larger clay fraction (between 15 and 6.5 GPa for clay fraction
3 between 28 and 50%).

4 Beside natural variability, the testing procedure adopted is another important
5 parameter to consider when comparing the data from various laboratories on COx
6 specimens. Tests have been run in both saturated and unsaturated conditions with
7 drainage conditions not always described in enough detail. By running a series of
8 unconfined compression tests on COx specimens equilibrated at various suctions
9 between 2.7 and 155.2 MPa (by using saturated saline solutions), Pham et al. [13]
10 confirmed the sensitivity of the COx claystone to changes in water content already
11 quoted by Chiarelli et al. [8], Zhang and Rothfuchs [9] and more recently by Zhang et
12 al. [23]. They obtained trends comparable to that evidenced by Valès et al. [12] on the
13 Tournemire shale, with significant increase in strength in drier states. The unconfined
14 compression strengths that Pham et al. [13] obtained at failure varied between 27 MPa
15 in a state close to saturated under a 98% relative humidity (suction 2.7 MPa, water
16 content 5.24%, degree of saturation not given) and 58 MPa in a much drier state under a
17 32% relative humidity (suction 155.2 MPa, water content 1.65%, degree of saturation
18 not given).

19 Prior to inspect further experimental data, it was found useful to present the
20 technical procedures used and published in the literature including the depth at which
21 specimens were extracted, the size of the specimen, their porosity, water content,
22 degree of saturation, testing rate and drainage length (an important parameter with
23 respect of drainage conditions). The data obtained in the works of Chiarelli [7] and
24 Chiarelli et al. [8], Zhang and Rothfuchs [9], Pham et al. [13] and Hu et al. [11] are
25 presented in Table 2. One can see that various sizes of triaxial specimens have been

1 used, the smallest being the 20 × 20 mm cylindrical specimen used by Hu et al. [11],
2 the longest one being the 100 mm high and 35 mm diameter used by Chiarelli [7] and
3 Chiarelli et al. [8]. Pham et al. [13] used a specimen of 72 mm in height and 36 mm in
4 diameter whereas Zhang and Rothfuchs [9] used a slightly larger specimen (40 mm in
5 diameter and 80 mm in length). Both sizes are close to standard triaxial specimens of 38
6 mm in diameter and 76 mm in height.

7 Whenever carried out, the saturation procedure has not always been described in
8 details by the authors. Some values of degree of saturation are given, that correspond to
9 the initial one as obtained when receiving the specimen in the laboratory (i.e. between
10 73 and 100 % for Chiarelli [7] and Chiarelli et al. [8] who tested their specimens at their
11 initial degree of saturation). The smallest degree of saturation was obtained after drying
12 to investigate the effects of change in water content on the shear strength (1.65% by
13 Pham et al. [13] and 2.8% by Zhang and Rothfuchs [9]). Although they did not
14 comment about their saturation procedure, Zhang and Rothfuchs [9] obtained almost
15 fully saturated specimens at $S_r = 99\%$. On their small specimen, Hu et al. [11] achieved
16 complete saturation by imposing a 1.5 MPa back-pressure on the bottom of the
17 specimen until monitoring the same value on the top. The change with time of the pore
18 pressure measured at the top of the specimen indicated that full saturation occurred
19 after 70 hours in the 20 mm high specimen.

20 The drainage conditions imposed during the tests are not always described in
21 detail. It seems that most often drainage was ensured by porous discs on top and bottom
22 of the specimens. The other important parameter is the strain rate imposed, that varies
23 between the largest value of $6.5 \times 10^{-6} \text{ s}^{-1}$ (Zhang and Rothfuchs [9]) in undrained tests
24 down to 10^{-7} s^{-1} in Hu et al [11] in drained tests with a drainage length of 10 mm. The
25 corresponding speeds are also given in Table 2 in $\mu\text{m}/\text{mn}$, knowing that drained tests in

1 clayey soils (permeability of 10^{-17} m^2) are typically conducted at a speed of $1 \mu\text{m}/\text{mn}$
2 with a 19 mm drainage length equal to the specimen radius, thanks to lateral drainage
3 allowed by filter papers placed all around the sample. In this regard, given the claystone
4 average permeability of 10^{-20} m^2 , it seems that drainage was not ensured in the tests of
5 the Table run with speeds larger than $3\mu\text{m}/\text{mn}$ and drainage lengths larger than 40 mm.
6 Conversely, the strain rate of 10^{-7} s^{-1} (speed of $0.12 \mu\text{m}/\text{mn}$) adopted by Hu et al. [11]
7 with a drainage length of 10 mm should ensure satisfactory drainage.

8 Note that, in fully saturated clayey soil specimens, imperfect drainage leads to
9 over-estimate the shear strength. When specimens are not fully saturated, things are
10 different because water is under a suction state and generally keeps retained by the
11 specimen with only air exchanges. The shear strength properties can then be over-
12 estimated by partial saturation.

13 Fig. 1 presents a synthesis of the shear strength data from tests of Table 2 from
14 the authors mentioned above, plotted in a diagram giving the shear stress at failure with
15 respect to the constant confining Terzaghi effective stress applied during the test. One
16 observes that the data of Chiarelli [7] at various depths with varying degree of
17 saturation exhibit more dispersion and are located clearly above other data, probably
18 because of partial saturation. The most coherent set of data is provided by Hu et al. [11]
19 on specimens EST30446 from vertical borehole in the URL at a depth of around 521.5
20 m, with good correspondence between drained and undrained saturated tests. The data
21 of Zhang and Rothfuchs [9] come from both UCS tests and two multistage undrained
22 tests on apparently saturated specimens (saturation procedure not described in the
23 paper). In perfectly saturated clayey soils, undrained triaxial tests carried out at various
24 confining stresses would provide a horizontal failure criterion providing only one value
25 of undrained shear strength. It is not the case here with a slope comparable to that

1 obtained in drained conditions. Imperfect saturation could be a reason why the criterion
2 is not horizontal. The data of Hu et al. [11] provide, adopting a Mohr Coulomb
3 criterion, a friction angle around 21° close to what could be obtained from that of
4 Zhang and Rothfuchs [9]. The data of Chiarelli [7], [8], more dispersed, would provide
5 higher friction angles.

6 The cohesion that would be obtained from Zhang and Rothfuchs [9]'s data (9
7 MPa, Fig. 1) is higher than that from Hu et al. [11], possibly due to partial saturation as
8 well. This is compatible with data on the shear strength properties of unsaturated soils
9 [24] that evidenced little effect of suction on the friction angle but significant effect on
10 the cohesion, the higher the suction, the higher the cohesion.

11 There is little published data on the thermal behaviour of claystones. In terms of
12 volume changes in clays, the important influence of overconsolidation, initially
13 evidenced by Hueckel and Baldi [2] on Boom clay and Pontida clay, was confirmed by
14 others (see for instance [4] on Boom clay and [5] on compacted clay). It is well
15 established that normally consolidated clays (that never supported any overburden
16 higher than what they supported when extracted) contract when heated under constant
17 load whereas overconsolidated clays (that supported during their geologic history an
18 overburden higher than what they were supporting when extracted, due for instance to
19 erosion of upper layers) tend to exhibit elastic thermal expansion. A combined dilating-
20 contracting behaviour can be observed on slightly overconsolidated clays, like for
21 instance Boom clay.

22 The volume changes of the COx claystone submitted to temperature elevation
23 under constant isotropic stress close to in-situ conditions was recently investigated in
24 fully saturated and fully drained conditions by Mohajerani et al. [19] by using the
25 hollow cylinder triaxial apparatus. They observed a thermal contraction, evidencing

1 behaviour comparable to that of normally consolidated clays. On the Opalinus clay,
2 Monfared et al. [18] observed a dilating-contracting behaviour with expansion up to a
3 temperature of 65° close to the maximum estimated temperature supported during its
4 geological history (65-70°C). Expansion was followed by contraction at higher
5 temperature (up to 80°C). Interestingly, a subsequent temperature cycle up to 80°C
6 exhibited thermal expansion, evidencing a thermal hardening phenomenon.

7 Zhang et al. [25] run at various temperatures (from 20 to 115°C) undrained
8 triaxial shearing tests (strain rate 10^{-7} s^{-1}) under constant 3 MPa confining stress on
9 Opalinus clay specimens with bedding planes inclined of 30-40°. The specimens had an
10 initial degree of saturation of 88%. Zhang et al. [25] observed in such conditions a more
11 ductile behaviour at elevated temperature with clear decrease in strength due to
12 temperature elevation (maximum shear strength of 20 MPa at 20°C and of 5 MPa at
13 115°C). More recently, Zhang et al. [26] conducted triaxial micro-compression tests on
14 unsaturated standard triaxial specimens submitted to a relative humidity of around 74%.
15 They observed little sensitivity with respect to temperature in the stress strain curves
16 obtained between 20 and 95°C under a confining stress of 15 MPa (around twice the in-
17 situ effective stress), whereas a decrease in peak stress (with small sensitivity in the
18 elastic regime) was observed under a confining stress of 5 MPa (smaller than the in-situ
19 stress). Masri et al. [27] conducted a series of what they called “pseudo-drained”
20 triaxial shear tests at temperatures between 20 and 250°C under three confining
21 pressures (5, 10 and 20 MPa) at an axial strain rate of 10^{-6} s^{-1} on specimens not fully
22 saturated (degree of saturation not provided). Specimens of 37 mm in diameter and
23 74 mm in height were bored with air pressure from cubic blocks extracted in the
24 Tournemire URL (France). Their observations are comparable to that made by Zhang et
25 al. [25] on Opalinus clay, with significantly more ductile behaviour observed at

1 elevated temperature and peak stress decreasing from 90 MPa at 20°C down to 40 MPa
2 at 250°C (tests run with bedding perpendicular to specimen axis).

3 The two previous works indicate that there is a suspicion of having an increase in
4 ductility and a decrease in shear strength in claystones with elevated temperature.
5 However, due to obvious experimental difficulties, these results are based on tests that
6 have not been conducted under fully saturated and drained conditions. The necessity
7 and interest of exploring this issue with well adapted devices and procedures, as
8 proposed in this work, are hence confirmed.

9 **3. Experimental device**

10

11 *3.1 Description*

12 A global overview of the hollow cylinder triaxial cell specially designed to investigate
13 the thermo-hydro-mechanical behaviour of low permeability clays and claystones [16]
14 is presented in Fig. 2a that schematically shows the triaxial cell containing the hollow
15 cylinder specimen (external diameter $D_{ext} = 100$ mm, internal diameter $D_{int} = 60$ mm,
16 height $H = 70-80$ mm). Note that the same confining pressure is applied along both the
17 external and internal lateral faces of the specimen thanks to a connection between these
18 two volumes. As shown in Fig. 2a-b, a major advantage of this device is provided by
19 the two lateral drainages in the inner and outer walls of the hollow cylinder specimen.
20 These drainages are made up of two geotextiles bands placed along the specimen, with
21 no contact between the bands and the upper and lower drainages. These lateral
22 drainages reduce the specimen drainage length down to half the thickness of the hollow
23 cylinder, i.e. 10 mm. Satisfactory drainage conditions are achieved during mechanical
24 and thermal loading provided the strain rate and temperature elevation rate is small
25 enough. Numerical calculations carried out by Monfared et al. [18] showed that a stress

1 rate of 0.5 kPa/mn ensured satisfactory drainage in hollow cylinder specimens with
2 permeability as low as 10^{-20} m².

3 The axial force is applied by using an integrated piston specially developed (Fig.
4 2a). The displacements of the piston are controlled by a pressure-volume controller
5 (maximum pressure of 60 MPa) connected to the upper chamber of the piston. The
6 applied axial force is directly measured by a local immersed force sensor fixed at the
7 bottom end of the piston. It can also be estimated from the pressure exerted and
8 measured by the PVC.

9 Fig. 2b shows a schematic view of the hydraulic connections between the
10 specimen, the pressure-volume controllers (PVC) and the pressure transducers (PT).
11 PVC1 is used to apply the confining pressure whereas the other three PVCs are used to
12 apply and control the pore fluid pressure. The device also comprises a system used to
13 monitor local strains composed of two axial and four radial local displacement
14 transducers (LVDTs, precision $\pm 1\mu\text{m}$, Fig. 2c).

15 The heating system consists of a heating electric belt placed around the cell with
16 a temperature regulator with a precision of $\pm 0.1^\circ\text{C}$. Temperature is measured inside the
17 cell close to the specimen by a thermocouple. The cell is covered by insulating layer in
18 order to limit heat exchanges with the environment.

19 *3.2. Preliminary resaturation procedure*

20 As shown by Monfared et al. [16], an interesting feature of the hollow cylinder
21 triaxial cell is its ability to ensure good initial saturation of specimens of very low
22 permeability (around 10^{-20} m² in the case of the COx claystone) within a reasonable
23 period of time thanks to a drainage path equal to half the thickness of the hollow
24 cylinder. Proper preliminary resaturation of specimens that have been desaturated
25 during coring, conservation, transport and machining in the laboratory is essential. The

1 initial degree of saturation of the specimens appears to be an important parameter with
2 respect to specimen quality.

3 As recalled by Delage et al. [28] on the Boom clay, Monfared et al. [18] on the
4 Opalinus clay and Mohajerani et al. [29] on the COx claystone, it is important to
5 resaturate specimens of swelling clays under stress conditions close to in-situ ones in
6 order to avoid further perturbation due to swelling during hydration. The in-situ state of
7 stress at the level of the Bure URL has been investigated in detail by Wileveau et al.
8 [30] who provided the following values: vertical total stress $\sigma_v = 12.7$ MPa, minor
9 horizontal total stress $\sigma_h = 12.4$ MPa and major horizontal total stress $\sigma_H = 16.2$ MPa,
10 situ pore pressure $u = 4.7$ MPa. Mohajerani et al. [29] used a confining stress of 12
11 MPa and a pore pressure of 4 MPa, resulting in a Terzaghi effective stress of 8 MPa. So
12 as to reduce the risk of leaks due to possible perforation of the neoprene jacket under
13 high stresses, it was preferred here to adopt the same Terzaghi 8 MPa effective stress
14 value with lower values, i.e. a 9 MPa confining pressure and a 1 MPa pore pressure.

15 Fig. 3 shows the volume changes calculated from the water injected from the back
16 pressure PVCs compared to that monitored by local LVDT measurements during the
17 saturation phase of tests T3 (specimen EST28514, porosity $\phi = 17.6\%$, initial degree of
18 saturation $S_{ri} = 85\%$) and T6 (specimen EST45407, $\phi = 13.5\%$, $S_{ri} = 39\%$). The curves
19 show that the stabilization of the water injected and of the volume changes derived
20 from the local LVDTs occurred after two days in both cases. The higher volume change
21 obtained from the water injected from the PVC is due to the effect of the water volume
22 needed to saturate the porous elements in contact with the specimen, i.e. the lateral
23 geotextiles and the upper and lower porous discs. One can also observe that the water
24 injected from PVCs in test T6 (7.4%, $S_{ri} = 39\%$, Fig. 3b) is significantly larger than that
25 injected in test T3 (2.3%, $S_{ri} = 85\%$, Fig. 3a) because of the significantly smaller initial

1 degree of saturation in T6. A slightly larger swelling is monitored by the LVDTs in test
2 T3 (1.18% compared to 1.04% for T6), perhaps linked to the difference in clay fraction
3 between both specimens, with a larger clay fraction in the more porous T3 specimen
4 (porosity 17.6%).

5 *3.3. Radial permeability tests*

6 Steady state permeability measurements were carried out by applying a radial
7 pressure gradient across the specimen and by measuring inflow and outflow fluxes by
8 using the PVCs. Permeability tests were carried out on specimens with an initial
9 backpressure of 1 MPa by closing the valves connected to the top and bottom of the
10 specimen and by applying a pressure excess of 0.5 MPa through the external geotextile
11 while maintaining the internal pressure equal to 1 MPa.

12 The radial intrinsic permeability k_r (m^2) was calculated using the flow rates as
13 follows:

$$14 \quad k_r = \frac{Q\mu_w \ln(R_{ext} / R_{int})}{2\pi h \Delta u} \quad (1)$$

15 where Q is the water flow; μ_w the water viscosity (equal to 8.90×10^{-4} Pa.s at 25°C and
16 3.55×10^{-4} Pa.s at 80°C), R_{ext} and R_{int} the external and internal specimen radius,
17 respectively ($R_{ext} = 50$ mm; $R_{int} = 30$ mm); h the flow height ($h = 50$ mm); and Δu the
18 pressure difference between the inner and outer walls of the specimen ($\Delta u = 0.5$ MPa).

19 *3.4. Comments on the hollow cylinder device*

20 As commented previously, the advantages of the hollow cylinder device in term of both
21 resaturation duration and drainage conditions are provided by the short drainage length
22 equal to half the thickness of the cylinder (10 mm), thanks to the external and internal
23 lateral drainages. Compared to small triaxial specimens that also have short drainage
24 paths, the hollow cylinder configuration also allows the monitoring of axial and radial

1 local strains thanks to the larger specimen size. Also, this specific configuration allows
2 perform radial permeability tests in sheared specimens by forcing the water flux in the
3 network of shear bands. This ability has proven being quite useful in the investigation
4 of the self-sealing properties of the Boom clay [17] and of the Opalinus clay [31].
5 However, based on the experience gained in the previous studies during the TIMODAZ
6 European project (see Li et al. [32]) and also gained in previous investigations carried
7 out on the COx clay [19], some difficulties have been met in link with the difficulty of
8 machining 100 mm diameter hollow cylinder specimens (see Monfared et al. [17] for
9 more details). This firstly requires large cores of 100 mm in diameter, which is
10 expensive and not so common. Most cores presently extracted from the Bure URL by
11 Andra have a diameter of 80 mm. In this study, good quality hollow cylinder specimens
12 were obtained on a lathe specially devoted to trimming claystone specimen at CEA, the
13 French research institute in nuclear energy.

14 For this reason of availability of large diameter cores, the tests of this program
15 had to be carried out on available specimens from different origins and initial
16 characteristics, as shown in Table 1.

17 *3.5. Experimental program*

18 Five different loading paths were performed on six hollow cylinder specimens that were
19 machined with the axis perpendicular to bedding to investigate some aspects of the
20 thermo-hydro-mechanical behaviour of the COx claystone, as described in Table 3 and
21 in Fig. 4. The same stress path was followed for tests T2 and T3. All specimens were
22 previously saturated as described in section 3.2. Tests T1, T2, T3 and T4 were carried
23 out along paths aimed at investigating the shear response at 25°C, as shown in Fig. 4.
24 To do so, constant confining pressure tests were carried out at 25°C close to in-situ

1 condition ($\sigma_3 = 9$ MPa, $u = 1$ MPa), around half the in-situ condition ($\sigma_3 = 5$ MPa,
2 $u = 1$ MPa) and twice the in-situ condition ($\sigma_3 = 17$ MPa, $u = 1$ MPa).

3 The same program was planned at 80°C but the test planned under twice the in-
4 situ stress condition failed due to leakage and no more hollow cylinder specimen was
5 available to do it again. The tests under constant confining stress finally performed at
6 80°C were test T5 on specimen EST45414 (like T1) under stress conditions close to in-
7 situ ($\sigma_3 = 9$ MPa, $u = 1$ MPa) and test T5 on specimen EST 45407 under half the in-situ
8 condition ($\sigma_3 = 5$ MPa, $u = 1$ MPa).

9 The tests carried out under half the in-situ condition are expected to swell during
10 the stress release from the initial in-situ condition under which they have been
11 resaturated (see Mohajerani et al. [33]). Particular care was put in following this
12 swelling phase to make sure that the specimen reached equilibrium in water content. It
13 seemed that this stress path was preferable to get a relevant response, compared to the
14 standard stress path in which the specimen would have been directly submitted to the
15 desired stress state prior to perform the resaturation procedure.

16 Steady state permeability tests were also planned in some tests. Their interest is
17 to provide further insight on the effects of temperature, compression and swelling on
18 the permeability. Successful radial steady state permeability tests were performed in
19 test T6 at points B (after resaturation), C (after swelling) and D (after heating the
20 swelled specimen up to 80°C).

21 **4. Experimental results**

22

23 *4.1. Test at 25°C*

24 Test T1, a drained shear test at constant confining stress close to the in-situ
25 effective stress, was carried out with a constant axial displacement rate of 0.4 $\mu\text{m}/\text{mn}$
26 while measuring the strength by using both the immersed force gauge and the pressure

1 measurement provided by the PVC applying the axial force. One observes in Fig. 5 the
2 changes in axial, radial and volumetric strains with respect to the shear stress ($q = \sigma_1$
3 $- \sigma_3$). The curves show that the maximum value of the shear stress at peak is 23 MPa. A
4 good correspondence was observed between the force measured by the immersed force
5 gauge and that obtained from by the external measurement provided by the CPV
6 pressure applied on the piston chamber (not given here). The peak is reached at 0.62%
7 of local axial strain and 0.24% of local radial strain. Note that the two axial LVDTs
8 transducers have not moved at the beginning of the test, up to 4 MPa of shear stress.

9 Fig. 5 also shows that the axial strain at peak found by external LVDT is of the
10 order of 1.45%, significantly higher than the 0.62% strain monitored by the local axial
11 LVDT. This difference is due to the non-negligible effects of the compressibility of the
12 whole system of axial stress application. It shows that Young's modulus obtained from
13 external axial measurements might be significantly underestimated.

14 A contracting dilating behaviour is observed before reaching the peak with a
15 transition observed at 16.5 MPa. The post-peak response is controlled by strain
16 localisation and the response of the resulting discontinuity observed after failure.
17 Indeed, one observes on the photographs of the specimen at the end of the test (Fig. 6) a
18 network of shear bands with an inclination of 66° with respect to horizontal. One also
19 notes the darker colour of the specimen due to full saturation, compared to the initial
20 clearer grey colour of COx specimens.

21 Once resaturated under in-situ stress condition, the specimens of tests T2, T3
22 and T6 were unloaded to a stress state close to half the in-situ one ($\sigma_3 - u = 4$ MPa) in
23 drained condition with the four drainages connected to a PCV imposing a backpressure
24 $u = 1$ MPa. To do so, the confining pressure was decreased from 9 to 5 MPa at a slow
25 rate of 1 kPa/mn. During this phase, the specimen volume monitored by LVDTs

1 transducers increased by 1.21%, 1.12% and 0.63% after 12 days for tests T2, T3 and T6
2 respectively. In a standard fashion, more swelling was observed in the direction
3 perpendicular to bedding as seen in Fig. 7. The larger swelling observed in the
4 specimens of tests T2 and T3 of larger porosity (16.5 and 17.6% respectively) confirm
5 the effect of a larger clay fraction, as previously mentioned in Section 3.2 when
6 describing the resaturation phase.

7 Specimens were afterwards maintained under a confining pressure of 5 MPa for
8 a few days in order to see possible swelling under a constant mean effective stress
9 lower than the in-situ one (~8 MPa). A volumetric swelling ratio of 0.013%/day,
10 0.022%/day and 0.010%/day were measured by LVDTs for T2, T3 and T6 respectively.

11 The specimens of tests T2 ($\phi = 16.5\%$) and T3 ($\phi = 17.6\%$) were then sheared
12 under a constant confining stress equal to half the in-situ effective stress (4MPa) in
13 drained conditions with axial displacement rates of 0.5 $\mu\text{m}/\text{mn}$ and 0.4 $\mu\text{m}/\text{mn}$
14 respectively. Fig. 8 shows the axial, radial and volumetric strains changes with respect
15 to shear stress for both specimens. A peak strength value of 10.5 MPa at axial and
16 radial strains of 1.06% and 0.24% respectively is observed for T2. A peak strength
17 value of 10.3 MPa at axial and radial strains of 1.01% and 0.33% respectively was
18 obtained for T3, showing good repeatability in the response of those two specimens of
19 comparable porosity.

20 Fig. 9 presents the axial, radial and volumetric strain with respect to the shear
21 stress for specimen of test T4 under a constant value of confining stress close to twice
22 the in-situ one (8 MPa) with a peak strength at 25.5 MPa at axial and radial strains of
23 1.15% and 0.60% respectively.

24

25

1 4.2. Drained heating test

2 Once resaturated under an effective confining stress close to in-situ (cell
3 pressure $\sigma_3 = 9$ MPa, back pressure $u = 1$ MPa), a drained heating test (T5) was carried
4 out under the same constant effective stress on specimen EST45414 ($\phi = 13\%$). A
5 comparable test (T6) was carried out under half the in-situ effective stresses
6 ($\sigma_3 = 5$ MPa, $u = 1$ MPa) on specimen EST45407 ($\phi = 13.5\%$). To do so, the cell was
7 slowly heated up to 80°C with a slow heating rate of 0.5°C/h [4, 18], keeping the four
8 drainage open (top, bottom, lateral inner and outer).

9 Fig. 10 presents the thermal local axial, radial and volumetric strains obtained
10 from LVDT measurements during the drained heating test. As already observed by
11 Mohajerani et al. [19], they show that the drained thermal volumetric response of the
12 COx claystone under constant in-situ stress is characterized by a contraction occurring
13 from the beginning of the test, with axial strains slightly larger than radial strains,
14 showing slight degree of anisotropy in the thermal response. This anisotropy shows that
15 the direction perpendicular to bedding (axial strains) is somewhat more sensitive than
16 that parallel to bedding (radial strains). At 80°C , the axial strain is equal to 0.06%
17 (characterised by a slope $C_{TL} = 1.14 \times 10^{-5} \text{ }^\circ\text{C}^{-1}$), compared to 0.06% for the radial strain
18 (characterised by a slope $C_{TL} = 1.06 \times 10^{-5} \text{ }^\circ\text{C}^{-1}$), resulting in a slope of $3.16 \times 10^{-5} \text{ }^\circ\text{C}^{-1}$
19 for the volume changes.

20 Fig. 11 shows the thermal response obtained during the drained heating test
21 carried out under half the in-situ effective stresses (test T6). The changes in axial strain
22 also indicate a continuous and almost linear contraction with a slope (perpendicular to
23 bedding) $C_{TL} = 0.96 \times 10^{-5} \text{ }^\circ\text{C}^{-1}$. In this test, no more change was observed in radial
24 strain above 37°C , due to some friction effect in the radial LVDT. However, the
25 changes in axial strain observed up to 37°C are comparable to the radial ones, with a

1 slope (parallel to bedding) $C_{T\parallel} = 0.77 \times 10^{-5} \text{ }^\circ\text{C}^{-1}$. Based on this value, a volumetric
2 thermal contraction coefficient of $2.49 \times 10^{-5} \text{ }^\circ\text{C}^{-1}$ is obtained. Thermal contraction
3 appears to be slightly smaller under half in-situ stress conditions than under in-situ
4 ones.

5 *4.3. Shear tests at 80°C*

6 Once the drained heating phase completed, specimens of tests T5 and T6 were
7 submitted to drained shearing with a constant axial displacement rate of 0.3 $\mu\text{m}/\text{min}$ and
8 0.4 $\mu\text{m}/\text{min}$ respectively. Fig. 12a shows that the shear stress at 80°C under in-situ stress
9 condition reached a peak value of 20 MPa at 0.75% of axial strain and 0.31% of radial
10 strain in test T5. The volume change is characterized by a contracting behaviour, at the
11 beginning (up to a 14.6 MPa), followed by a dilation phase up to the peak. As
12 previously, Fig. 12a shows that the axial strain found by an external measurement at
13 peak is about 1.2%, significantly higher than that given by the local measurement.

14 The shear test at 80°C carried out under half the in-situ effective stresses (4MPa)
15 is presented in Fig. 12b. This curves shows that the shear stress reaches its maximum
16 value of 16 MPa at 1.25% and 0.35% of axial and radial strain respectively.

17 *4.4. Failure criterion*

18 All the peak values (q_{max}) obtained in the previous tests are brought together in Fig. 13
19 together with the data of Hu et al. [11] that also concern fully saturated and drained
20 tests. The tests run at 25°C on three specimens with a porosity of 16-17% are located
21 along a line parallel to that obtained at 80°C on specimens with porosity around 13%.
22 There is unfortunately only one point at 25°C for a specimen with porosity around 13%.
23 The failure points at 80°C obtained under in-situ effective stress from a specimen with
24 porosity close to 13% is located slightly below that at 25°C. This set of data will be
25 further commented in the Discussion section.

1 4.5. Radial permeability tests

2 Radial permeability tests were carried out in some cases to investigate the effects of
3 volume changes and of temperature on water transport. Given that specimens were
4 machined with axis perpendicular to bedding, the flow of water during radial
5 permeability tests is governed by the permeability parallel to bedding. As described in
6 Section 3.3, tests were carried out by applying a 1.5 MPa pore pressure on the external
7 lateral face of the hollow cylinder while maintaining the pressure on the internal face
8 equal to the initial back pressure of 1 MPa. The confining pressure was kept equal to
9 9 MPa.

10 The inflow and outflow curves monitored by the upstream and downstream
11 PVCs for the test after resaturation under in-situ stress conditions of the specimen of
12 test T6 (porosity 13.6%) are presented in Fig. 14 (in which the Q final inflow and
13 outflow are indicated). Actually, a tiny leak was observed on the upstream PVC when
14 bringing back the pressure from 1.5 to 1 MPa at the end of the test. This leak (estimated
15 by 23% of the monitored inflow at point B) was accounted for and inflow curves
16 corrected accordingly (note however that the correction was made under 1 MPa
17 whereas tests were carried out under 1.5 MPa). Less confidence is hence given to
18 inflow curves compared to outflow curve that were not affected by any leak.

19 Fig. 14 shows that, once the upstream injection starts, it was necessary to wait
20 for 30 minutes before monitoring any outflow with the downstream PVC. This period
21 of time was necessary to install steady state conditions and to reach the new effective
22 stress state resulting from the 1.5 MPa pore pressure exerted along the external face of
23 the specimen. By applying Darcy's law on the outflow observed at the end of test
24 ($Q = 3.35 \times 10^{-12} \text{ m}^3/\text{s}$), a radial permeability of $0.9 \times 10^{-20} \text{ m}^2$ is obtained. That
25 obtained from the inflow value ($Q = 3.88 \times 10^{-12} \text{ m}^3/\text{s}$) is close, although slightly larger

1 ($k = 1.1 \times 10^{-20} \text{ m}^2$), confirming the good quality of the measurement (with satisfactory
2 correction of the upstream leak).

3 Fig. 14b shows the changes in volume obtained from water exchanges
4 (calculated from the upstream and downstream PVCs data) and from local LVDTs
5 measurements. For some reason, the two curves are not in good correspondence during
6 the first 14 hours with LVDTs indicating fast swelling during the first two hours. Both
7 curves afterwards correspond and indicate that the specimen slightly swells (0.034%
8 after 27 hours with a final swelling rate of $4.3 \times 10^{-4} \text{ h}^{-1}$). The amount of water adsorbed
9 during the test explains the slight difference between the inflow and outflow data, and
10 between the two calculated permeabilities.

11 Another radial permeability test was carried out in test T6 after releasing the
12 confining stress to half the in-situ value to investigate the effect of the resulting 0.63%
13 swelling (Point C, Fig. 4). Inflow and outflow data (Fig. 15a) are comparable to that
14 observed above with no outflow during the first hour, providing at the end of test radial
15 permeability values of $1.2 \times 10^{-20} \text{ m}^2$ and $1.6 \times 10^{-20} \text{ m}^2$, respectively. These values are
16 slightly higher than before stress release and are related to the 0.63% swelling. The
17 PVC volume change curve (Fig. 15b) provides a slightly larger volume change value
18 than LVDTs at end of test. The final swelling rate is $5.9 \times 10^{-4} \text{ h}^{-1}$.

19 The data of the permeability test finally carried out after drained heating (Point D,
20 Fig. 4, test T6, thermal contraction 0.106%, see Fig. 11) are presented in Fig. 16 a and
21 b. This test had to be stopped after only 7 hours with a final swelling rate of 3.7×10^{-3}
22 h^{-1} . Even after a shorter period of time, swelling is close to 0.07%, i.e. almost twice that
23 observed in the two previous tests at 25°C, indicating possible enhancing of swelling
24 with elevated temperature. Compared to previous tests at 25°C, larger fluxes are
25 obtained ($Q_{inflow} = 2.52 \times 10^{-11} \text{ m}^3/\text{s}$ and $Q_{outflow} = 1.58 \times 10^{-11} \text{ m}^3/\text{s}$). Here, the

1 difference between inflow and outflow is larger than previously. Given that the
 2 upstream leak correction done at 25°C could not be valid here, only the outflow curve
 3 is considered to provide an (intrinsic) permeability value equal to $1.8 \times 10^{-20} \text{ m}^2$. As
 4 further commented in the Discussion session, larger fluxes are related to the decrease in
 5 water viscosity. A larger permeability is observed at 80°C in spite of a slight porosity
 6 reduction.

7 **4. Discussion**

8 *4.1 Elastic response*

9 A series of triaxial tests have been conducted on COx claystone specimens
 10 along various thermo-hydro-mechanical paths (Fig. 4) in fully saturated and drained
 11 conditions by using the hollow cylinder device. Although all of the tests initially
 12 planned were not successful because of the technical difficulty of getting hollow
 13 cylinder specimens and of running hollow cylinder triaxial tests, some conclusions can
 14 be drawn from the data obtained.

15 The various shear stress/axial strain curves obtained on specimens trimmed with axis
 16 perpendicular to bedding allow the determination of some elastic constants that partly
 17 describe the transverse isotropic elastic behaviour of the COx claystone. As described
 18 by Cheng et al. [34], the stress-strain elastic relationship for a transverse isotropic
 19 material is as follows:

$$20 \begin{pmatrix} d\varepsilon_1 \\ d\varepsilon_2 \\ d\varepsilon_3 \end{pmatrix} = \begin{pmatrix} \frac{1}{E_1} & -\frac{\nu_{21}}{E_2} & -\frac{\nu_{21}}{E_2} \\ -\frac{\nu_{12}}{E_1} & \frac{1}{E_2} & -\frac{\nu_{23}}{E_2} \\ -\frac{\nu_{12}}{E_1} & -\frac{\nu_{23}}{E_2} & \frac{1}{E_2} \end{pmatrix} \begin{pmatrix} d\sigma_1 \\ d\sigma_2 = 0 \\ d\sigma_3 = 0 \end{pmatrix} \quad (2)$$

21 with $d\sigma_2 = d\sigma_3 = 0$ under “triaxial” conditions and where ν_{23} and E_2 are the Poisson
 22 ratios and Young modulus in the plane of isotropy (2-3), and ν_{12} , ν_{21} and E_1 are the

1 Poisson ratio and Young modulus in the plane perpendicular to the plane of isotropy.
2 The Young modulus and Poisson ratio perpendicular to bedding can be calculated by
3 using the data of the drained triaxial test using Eq. (3) and Eq. (4).

$$4 \quad \frac{d\varepsilon_1}{d\sigma_1} = \frac{1}{E_1} \quad (3)$$

$$5 \quad \frac{d\varepsilon_2}{d\sigma_1} = -\frac{\nu_{12}}{E_1} \quad (4)$$

6 From the data of Fig. 5 under a confining stress close to in-situ (8 MPa Terzaghi
7 effective stress), a value $E_I = 3.2$ GPa is obtained from the shear stress-axial strain
8 curve for a mobilisation of 0.1% of axial strain, with $\nu_{12} = 0.30$ (Table 4). When the
9 confining stress has been released close to half the in-situ one, values $E_I = 1.5$ GPa and
10 1.3 GPa are deduced from tests T2 and T3 respectively with Poisson's ratio $\nu_{12} = 0.10$
11 in both cases (Fig. 8). Conversely, when the confining stress is increased to twice the
12 in-situ stress (test T4, Fig. 9), values of Young modulus and Poisson's ratio of 5.5 GPa
13 and 0.34, respectively, are obtained.

14 At 80°C, the estimated values of the E_I Young's modulus and the ν_{12} Poisson ratio
15 are $E_I = 3.4$ GPa and $\nu_{12} = 0.26$, respectively, under a confining stress close to in-situ.
16 Values $E_I = 1.4$ GPa and $\nu_{12} = 0.10$, respectively, were obtained under a confinement of
17 half the in-situ stress.

18 All the values obtained at 25 and 80°C are plotted together in Fig. 17 that clearly shows
19 that there is no effect of temperature on the elastic properties determined here (Young's
20 modulus E_I and Poisson coefficient ν_{12}). Similar comparison has been drawn by
21 Mohajerani et al. [19] from isotropic compression tests, showing no effect of
22 temperature (80°C) on the elastic compression parameters. The Young's modulus also
23 regularly increases with the effective confining stress. It is important to recall that all

1 the points tested here started from previous saturation under in-situ stress, with the
2 smaller confining stress at half in-situ stress (4 MPa) obtained by subsequent stress
3 release (and mobilisation of swelling). The Poisson ratio ν_{12} , equal to 0.30 at initial
4 state under in-situ stress (8 MPa) decreases to 0.10 when the confining effective stress
5 is released at 4 MPa, both at 25 and 80°C, confirming the independency of the elastic
6 parameters with respect to temperature. Conversely, ν_{12} only slightly changes from 0.30
7 to 0.34 when the confining effective stress is increased at 16 MPa. This could indicate
8 that the decrease observed when releasing the effective confining stress could be related
9 to the slight swelling mobilized, an hypothesis to further confirm.

10 It seems difficult to compare the data obtained here with published data that
11 appear to have generally been obtained based on other experimental procedure like for
12 instance, for the Young modulus, from unconfined compression tests under not fully
13 saturated conditions [13, 26]. Data on the Poisson ratio are less available.

14 *4.2 Thermal volume changes*

15 Two drained heating tests were performed to investigate the thermal volumetric
16 response of the COx claystone under stress conditions close to in-situ (mean Terzaghi
17 effective stress of 8 MPa) and to half the in-situ stress (mean Terzaghi effective stress
18 of 4 MPa). They confirmed the contracting behaviour already evidenced by Mohajerani
19 et al. [19], but with smaller contraction coefficient, as indicated in Table 5. Whereas
20 Mohajerani et al. [19] observed a significantly anisotropic thermal response with
21 thermal contraction coefficients of 3.15 and $6.50 \times 10^{-5} \text{°C}^{-1}$ parallel and perpendicular
22 to bedding, respectively, the contraction observed here is less marked and less
23 anisotropic with $C_{T\perp} = 1.15 \times 10^{-5} \text{°C}^{-1}$ perpendicular to bedding and $C_{T\parallel} = 1.06 \times 10^{-5}$
24 °C^{-1} parallel to bedding under in-situ stress. These values slightly decreased to
25 $C_{T\perp} = 0.96 \times 10^{-5} \text{°C}^{-1}$ and $C_{T\parallel} = 0.77 \times 10^{-5} \text{°C}^{-1}$ under half in-situ stress. This smaller

1 contraction under smaller stress is not surprising. A possible reason of the significantly
2 smaller contraction observed here could come from the differences in origin and in
3 porosity between the specimens, with Mohajerani et al.'s [19] specimen significantly
4 more porous (17.9% compared to around 13% here). More porous samples have larger
5 clay content and clay content is the driving force of thermal contraction, given that the
6 grains of quartz and calcite contained in the clay matrix simultaneously expand,
7 probably resulting in some thermal damage at the interface between the grains and the
8 clay matrix.

9 The COx claystone is known to have supported a maximum temperature of
10 50°C during its geological history [35]. Unlike what was observed in the Opalinus clay
11 by Monfared et al. [18], one does not observe here an initial thermal expansion up to
12 50°C. For some reason, the thermal hardening phenomenon observed on the Opalinus
13 clay is not observed here.

14 *4.3 Shear strength and temperature effects*

15 Fig. 13 shows the values of peak strength (q_{\max}) as a function of effective mean stress
16 p' for all of the tests carried out here, together with the data obtained by Hu et al. [11]
17 at 25°C under fully saturated conditions. The porosity of the specimens is also
18 mentioned, given that the specimens tested by Hu et al. [11] have a porosity of around
19 13%. The Figure shows that the failure shear stress at 25°C are reasonably well
20 organised with respect to their porosity, with good correspondence between tests T1
21 (EST45414) under in-situ confining stress ($T = 25^\circ\text{C}$, $p' = 8 \text{ MPa}$, $\phi = 13\%$,
22 $q_{\text{failure}} = 23 \text{ MPa}$) and the data obtained by Hu et al. [11] at a comparable value of
23 porosity and same temperature. The failure data obtained at 25°C with the specimens of
24 17% porosity are located below that at 13%, exhibiting smaller shear strength for more
25 porous specimens, in a standard fashion. All tests at 25°C (including Hu et al. [11] data)

1 are aligned along parallel lines that define a friction angle of 21° equal to that proposed
2 by Hu et al. [11]. There is a decrease in cohesion that makes the more porous specimen
3 weaker with a cohesion of 1.94 MPa at 17% compared to 4.2 MPa at 13%. Note
4 however that the shear strength data obtained here appear to be somewhat small with
5 respect to the data of undrained compression tests carried out for Andra by various
6 laboratories that provided undrained compression strengths (UCS) around 20 MPa
7 (Conil, personal communication). Indeed, Pham et al. [13] reported a UCS of 28 MPa
8 on a specimen not fully saturated tested under a 98% relative humidity. A possibility of
9 underestimating the shear strength by the size and shape of the specimens tested
10 (hollow cylinder here and small cylinder for Hu et al. [11]) might be considered.

11 The two points obtained at a porosity of 13% at a temperature of 80°C are
12 located slightly below the points at the same porosity and 25°C , indicating a slight
13 reduction in shear strength due to temperature. The slight difference observed is
14 actually in the range of the dispersion observed when testing COx specimens, and this
15 preliminary observation is of course to be confirmed by further fully saturated and
16 drained tests. This trend is however in agreement with previous suggestions taken from
17 the works of Zhang et al. [25] on the Opalinus clay and of Masri et al. [27] on the
18 Tournemire shale.

19 *4.4 Permeability tests*

20 Steady state radial permeability tests were performed by imposing a pore pressure
21 increase ($\Delta u = 0.5$ MPa) on the outer face while maintaining the pore pressure equal to
22 1 MPa on the inner face of the hollow specimen. Water exchanges were monitored by
23 using the PVCs and LVDTs were used to monitor local volume changes. In spite of
24 some differences observed in the transient phase during the set up of the new effective
25 stress conditions resulting from the application of the 1.5 MPa external pore pressure,

1 the comparison of volume change data from LVDT measurements and from the water
2 exchanges monitored by the PVCs was reasonably satisfactory (in spite of a tiny leak),
3 providing some confidence in the permeability values obtained.

4 The radial permeability values (parallel to bedding) obtained at various stages of
5 test T6 (points B, C and D in Fig. 4) are presented in Table 6. The values of
6 permeability adopted and discussed below are that obtained from the outflow curves. A
7 reference permeability value of $0.9 \times 10^{-20} \text{ m}^2$ was obtained under in-situ stress
8 conditions, a value in the range of magnitude of published data (more often measured
9 along the axial direction) for the COx claystone, between 10^{-20} and $10^{-22} \text{ m}^2 \text{ m}^2$ [33, 36,
10 37, 38].

11 A slight change from $0.9 \times 10^{-20} \text{ m}^2$ to $1.2 \times 10^{-20} \text{ m}^2$ was obtained after the
12 0.63% swelling due to stress release from in-situ to half the in-situ stress. After drained
13 heating at 80°C (with a thermal contraction of 0.12% followed by a swelling of 0.07%),
14 larger inflow and outflow were observed due to the increase in water viscosity (from
15 $8.90 \times 10^{-4} \text{ Pa.s}$ at 25°C to $3.55 \times 10^{-4} \text{ Pa.s}$ at 80°C). The permeability at 80°C appeared
16 to be slightly larger and equal to $1.8 \times 10^{-20} \text{ m}^2$. Although these first results should be
17 confirmed, they show that the permeability is not totally independent of temperature,
18 unlike what was previously observed on the Boom clay [39], with a slight increase with
19 temperature. Note that this tests also showed an enhancement of swelling with
20 temperature, with around twice more swelling at 80°C compared to 25°C under same
21 stress conditions.

22

23

24

25

1 **5. Conclusion**

2
3 Published data on the shear strength properties of the Callovo-Oxfordian
4 claystone exhibit some variability due to the natural variability of the deposit, to the
5 changes of the claystone characteristics with depth and also to the testing procedures
6 adopted. An inspection of published data indeed showed that the specimens tested came
7 from various boreholes and from various depths and that the testing procedures were
8 variable in terms of specimen saturation and drainage conditions. It is well known that
9 partial saturation and drainage overestimate the shear strength properties of the COx
10 claystone, and this seems to be somewhat linked to the variability observed in the
11 published data.

12 Few data are available about the thermal response of the COx claystone. The
13 tests carried out here were performed after careful saturation under in-situ stress
14 conditions and in fully drained conditions thanks to the use of a hollow cylinder triaxial
15 apparatus with reduced drainage length specially designed for testing low permeability
16 rocks. Triaxial tests were carried out at 25 and 80°C to get some preliminary insights on
17 the effects of temperature on the shear strength properties of the claystone. Also, some
18 steady state radial permeability tests were carried out at 25 and 80°C to investigate the
19 effect of temperature on the claystone permeability.

20 Although somewhat small with respect to the previous UCS data gathered by
21 Andra, the shear strength data obtained here are in good agreement with that of tests
22 also carried out in fully saturated and drained conditions by Hu et al. [11] on specimens
23 of the same porosity (13%). Some effects of the porosity have also been evidenced,
24 with smaller shear strength values obtained on specimens with higher porosity (17%).
25 The thermal contraction of the COx claystone upon heating under constant in-situ stress
26 evidenced by Mohajerani et al. [19] was confirmed. Subsequent shear tests at 80°C

1 showed little changes of the elastic parameters with temperature, confirming the
2 findings of Mohajerani et al. [19]. The preliminary results obtained in this work
3 evidenced a more ductile response and slightly smaller shear strengths of the COx
4 claystone at elevated temperature, in agreement with the few available published data
5 on shales and claystones. Finally, radial permeability tests performed parallel to
6 bedding demonstrated that the intrinsic permeability did not change significantly with
7 elevated temperature, the larger flow observed at 80°C during the test being mainly due
8 to the decrease in viscosity of water.

9 The preliminary data obtained here on temperature effects on the shear strength
10 behaviour of the COx claystone need to be further confirmed by complementary tests,
11 they however confirm some trends already observed on the COx claystone and on other
12 clay rocks. A better understanding of the thermo-hydro-mechanical response of
13 claystone will allow a better understanding and modelling of the coupled THM actions
14 that prevail in the close field once the exothermic wastes have been placed.

15

16 **6. Acknowledgements**

17 The authors are grateful to Andra who founded this work that is part of the PhD
18 work of the first author. Andra also provided the COx specimens tested in this work.

19
20
21
22
23
24
25
26
27
28
29
30
31
32

1 7. References

- 2
- 3 [1] ANDRA (2005). Synthesis argile: evaluation of the feasibility of a geological
4 repository in argillaceous formation. [http://www.andra.fr/international/
5 download/andra-international-en/document/editions/266va.pdf](http://www.andra.fr/international/download/andra-international-en/document/editions/266va.pdf)
- 6 [2] Hueckel T, Baldi G. Thermoplasticity of saturated clays: experimental
7 constitutive study. *Journal of Geotechnical Engineering* 1990; 116(12):1768–
8 1796.
- 9 [3] Hueckel T, Pellegrini R. Thermoplastic modeling of undrained failure of saturated
10 clay due to heating. *Soils Found* 1991; 31(3):1-16.
- 11 [4] Sultan N, Delage P, Cui YJ. Temperature effects on the volume change behaviour
12 of Boom clay. *Engineering Geology* 2002; 64(2-3):135-145.
- 13 [5] Cekerevac C, Laloui L. Experimental study of thermal effects on the mechanical
14 behaviour of a clay. *International Journal for Numerical and Analytical Methods
15 in Geomechanics* 2004; 28:209–228.
- 16 [6] Hueckel T, François B, Laloui L. Explaining thermal failure in saturated clays.
17 *Géotechnique* 2009; 59 (3):197-212.
- 18 [7] Chiarelli AS. Étude expérimentale et modélisation du comportement mécanique
19 de l'argilite de l'est. PhD thesis, Université Lille I ; 2000.
- 20 [8] Chiarelli AS, Shao JF, Hoteit N. Modeling of elastoplastic damage behavior of a
21 claystone. *International Journal of Plasticity* 2003; 19:23-45.
- 22 [9] Zhang CL, Rothfuchs T. Experimental study of the hydro-mechanical behaviour
23 of the Callovo-Oxfordian argillite. *Applied Clay Science* 2004; 26(1-4): 325-336.
- 24 [10] Hoxha D, Giraud A, Homand F, Auvray C. Saturated and unsaturated behaviour
25 modelling of Meuse-Haute-Marne argillite. *International Journal of Plasticity*
26 2007; 23:733–766.

- 1 [11] Hu DW, Zhang F, Shao JF. Experimental study of poromechanical behavior of
2 saturated claystone under triaxial compression. *Acta Geotechnica* 2014a; 9:207-
3 214.
- 4 [12] Valès F, Nguyen Minh D, Gharbi H, Rejeb A. Experimental study of the influence
5 of the degree of saturation on physical and mechanical properties in Tournemire
6 shale (France). *Applied Clay Science* 2004; 26:197–207.
- 7 [13] Pham QT, Vales F, Malinsky L, Nguyen Minh D, Gharbi H. Effects of
8 desaturation-resaturation on mudstone. *Physics and Chemistry of the Earth* 2007;
9 32:646–655.
- 10 [14] Yang D, Chanchole S, Valli P, Chen L. Study of the Anisotropic Properties of
11 Argillite Under Moisture and Mechanical Loads. *Rock Mechanics and Rock*
12 *Engineering* 2012; 46(2):247–257.
- 13 [15] Wu B, Tan CP, Aoki T. Specially designed techniques for conducting
14 consolidated undrained triaxial tests on low permeability shales. *International*
15 *Journal of Rock Mechanics and Mining Sciences* 1997; 34:3-4), paper No. 336.
- 16 [16] Monfared M, Delage P, Sulem J, Mohajerani M, Tang AM, De Laure E. A new
17 hollow cylinder triaxial cell to study the behaviour of geomaterials with low
18 permeability. *International Journal of Rock Mechanics and Mining Sciences*
19 2011; 48 (4):637-649.
- 20 [17] Monfared M, Sulem J, Delage P, Mohajerani M. On the THM behaviour of a
21 sheared Boom clay sample: Application to the behaviour and sealing properties of
22 the EDZ. *Engineering Geology* 2012; 124:47-58.
- 23 [18] Monfared M, Sulem J, Delage P, Mohajerani M. A laboratory investigation on
24 thermal properties of the Opalinus claystone. *International Journal of Rock*
25 *Mechanics and Rock Engineering* 2011b; 44(6):735-747.

- 1 [19] Mohajerani M, Delage P, Sulem J, Monfared M, Tang A.M, Gatmiri B. The
2 thermal volume change of the Callovo-Oxfordian claystone. *International Journal*
3 *of Rock Mechanics and Rock Engineering* 2014; 47:131-142.
- 4 [20] Gaucher G, Robelin C, Matray JM, Négrel G, Gros Y, Heitz JF, Vinsot A,
5 Rebours H, Cassagnabère, Bouchet A. ANDRA underground research laboratory:
6 interpretation of the mineralogical and geochemical data acquired in the
7 Callovian-Oxfordian formation by investigative drilling. *Physics and Chemistry*
8 *of the Earth* 2004; 29:55-77.
- 9 [21] Yven B, Sammartino S, Geroud Y, Homand F, Villieras F. Mineralogy, texture
10 and porosity of Callovo-Oxfordian claystones of the Meuse/Haute-Marne region
11 (eastern Paris Basin). *Mémoires de la Société géologique de France*, ISSN 0249-
12 7549 2007; 178: 73-90.
- 13 [22] Hu DW, Zhang F, Shao JF, Gatmiri B. Influences of Mineralogy and Water
14 Content on the Mechanical Properties of Argillite. *Rock Mechanics and Rock*
15 *Engineering* 2014b; 47:157-166.
- 16 [23] Zhang F, Xie SY, Hu DW, Shao JF, Gatmiri B. Effect of water content and
17 structural anisotropy on mechanical property of claystone. *Applied Clay Science*
18 2012; 69:79–86.
- 19 [24] Fredlund DG, Rahardjo H, Fredlund MD. *Unsaturated soil mechanics in*
20 *engineering practice*. 2012; Wiley, New-York.
- 21 [25] Zhang CL, Rothfuchs T, Su K, Hoteit N. Experimental study of the thermo-hydro-
22 mechanical behaviour of indurated clays. *Phys Chem Earth Parts A/B/C* 2007;
23 32(8–14):957–965.
- 24 [26] Zhang F, Hu DW, Xie SY, Shao JF. Influences of temperature and water content
25 on mechanical property of argillite. *European Journal of Environmental and Civil*

- 1 Engineering 2014; 18(2):173–189.
- 2 [27] Masri M, Sibai M, Shao JF, Mainguy M. Experimental investigation of the effect
3 of temperature on the mechanical behavior of Tournemire shale. *International*
4 *Journal of Rock Mechanics and Mining Sciences* 2014; 70:185–191.
- 5 [28] Delage P, Le TT, Tang AM, Cui YJ, Li XL. Suction effects in deep Boom clay
6 block specimens. *Géotechnique* 2007; 57(1):239–244.
- 7 [29] Mohajerani M, Delage P, Monfared M, Tang A.M, Sulem J, Gatmiri B. A
8 laboratory investigation of thermally induced pore pressures in the Callovo-
9 Oxfordian claystone. *International Journal of Rock Mechanics and Mining*
10 *Sciences* 2012; 52:112-121.
- 11 [30] Wileveau Y, Cornet FH, Desroches J, Blumling P. Complete in situ
12 stressdetermination in an argillite sedimentary formation. *Phys Chem Earth*
13 *A/B/C* 2007; 32(8–14):866–78.
- 14 [31] Monfared M, Sulem J, Delage P, Mohajerani M. Temperature and Damage
15 Impact on the Permeability of Opalinus Clay. *International Journal of Rock*
16 *Mechanics and Rock Engineering* 2014; 47:101–110.
- 17 [32] Li Y, Weetjens E, Sillen X, Vietor T, Li X, Delage P, Labiouse V, Charlier R.
18 Consequences of the thermal transient on the evolution of the damaged zone
19 around a repository for heat-emitting high-level radioactive waste in a clay
20 formation: a performance assessment perspective. *Rock Mechanics and Rock*
21 *Engineering* 2014; 47:3-19.
- 22 [33] Mohajerani M, Delage P, Monfared M, Tang A.M, Sulem J, Gatmiri B.
23 Oedometric compression and swelling behaviour of the Callovo-Oxfordian
24 argillite. *International Journal of Rock Mechanics and Mining Sciences* 2011;
25 48(4):606-615.

- 1 [34] Cheng A HD. Material coefficients of anisotropic poroelasticity. International
2 Journal of Rock Mechanics and Mining Sciences 1997; 34(2):199-205.
- 3 [35] Blaise T, Barbarand J, Kars M, Ploquin F et al. Reconstruction of low temperature
4 (<100 _C) burial in sedimentary basins: A comparison of geothermometer in the
5 intracontinental Paris Basin. Marine and Petroleum Geology 2013;
6 <http://dx.doi.org/10.1016/j.marpetgeo.2013.08.019>.
- 7 [36] Escoffier S. Caractérisation expérimentale du comportement hydro-mécanique
8 des argillites de Meuse/ Haute Marne. PhD thesis, INPL Nancy ; 2002.
- 9 [37] Escoffier S, Homand F, Giraud A, Hoteit N, Su K. Under stress permeability
10 determination of the Meuse/Haute-Marne mudstone. Engineering Geology 2005;
11 81:329–340.
- 12 [38] Delay J, Trouiller A, Lavanchy JM. Propriétés hydrodynamiques du Callovo-
13 Oxfordien dans l’Est du bassin de Paris : comparaison des résultats obtenus selon
14 différentes approches 2006 ; C.R. Geoscience 338.
- 15 [39] Delage P, Sultan N, Cui YJ. On the thermal consolidation of Boom clay.
16 Canadian Geotechnical Journal 2000; 37(2):343-354.
- 17

1	Tables
2	
3	
4	Table 1. Initial characteristics of the tested specimens.
5	
6	Table 2. Characteristics published tests about the shear properties of the COx claystone.
7	
8	Table 3. Experimental programme.
9	
10	Table 4. Evolution of the elastic parameters.
11	
12	Table 5. Thermal contraction coefficients.
13	
14	Table 6. Effect of swelling and temperature on the COx claystone permeability (T6,
15	porosity 13.5 %).
16	
17	
18	
19	
20	
21	
22	
23	
24	
25	
26	
27	
28	
29	
30	
31	
32	
33	
34	
35	
36	
37	
38	
39	
40	
41	
42	
43	
44	
45	
46	
47	
48	
49	
50	

1 Figures
2
3
4 Fig. 1. Published shear strength data of the COx claystone.
5
6 Fig. 2. (a): Hollow cylinder triaxial cell, (b): Scheme of the hydraulic connections, (c):
7 Local strain measurement system.
8
9 Fig. 3. Volume changes and water exchanges during resaturation phase, (a): test T3,
10 (b): test T6.
11
12 Fig. 4. Thermo-hydro-mechanical paths followed during the tests carried out.
13
14 Fig. 5. Drained shear test under in-situ effective stresses at 25°C, test T1.
15
16 Fig. 6. COx claystone at the end of the test T1.
17
18 Fig. 7. Drained isotropic unloading phase, (a): T2, (b): T3, (c): T6.
19
20 Fig. 8. Drained shear test under half in-situ effective stresses at 25°C, (a): test T2, (b):
21 test T3.
22
23 Fig. 9. Drained shear test under twice in-situ effective stresses at 25°C, test T4.
24
25 Fig. 10. Axial, radial and volumetric strains measured during a drained heating test
26 (0.5°C/h) under in-situ effective stresses, test T5.
27
28 Fig. 11. Axial, radial and volumetric strains measured during a drained heating under
29 half in-situ effective stresses, test T6.
30
31 Fig. 12. Drained shear test at 80°C, (a): test T5, (b): test T6.
32
33 Fig. 13. Shear strength of all tests carried out in the plan q-p'.
34
35 Fig. 14. Radial permeability test at point B, after resaturation T6, (a): inflow and
36 outflow, (b): volume change.
37
38 Fig. 15. Radial permeability test at point C, after swelling T6, (a): inflow and outflow,
39 (b): volume change.
40
41 Fig. 16. Radial permeability test at point D, after heating T6, (a): inflow and outflow,
42 (b): volume change.
43
44 Fig. 17. Elastic parameters, (a): Young's modulus, (b): Poisson coefficient.
45
46
47
48
49
50

Table 1

Table 1. Initial characteristics of the tested specimens.

Specimen	Ref. Core	Depth (m)	Height (mm)	Water content (%)	Dry unit mass (Mg/m ³)	Porosity (%)	Degree of saturation (%)	Suction (MPa)
S1	EST45414	498	73.13	2.11	2.35	13.0	38	109
S2	EST30734	612	73.95	5.88	2.26	16.5	80	31
S3	EST28514	477	75.00	6.76	2.21	17.6	85	
S4	EST28518	479	71.02	6.10	2.20	17.8	80	34
S5	EST45407	499	72.60	2.27	2.34	13.5	39	

Table 2

Table 2. Characteristics published tests about the shear properties of the COx claystone.

Authors	N° Specimen	Depth (m)	Spec. height (mm)	Spec. diameter (mm)	Porosity (%)	Water content (%)	Degree of saturation (%)	Type of test	Testing rate (s ⁻¹) $\mu\text{m}/\text{mn}$ Drainage length H
Chiarelli (2000), Chiarelli et al. (2003)	EST 02172	451-467	100	35	11.5* <i>Est. 15.3</i>	4 – 5.7	73 – 93	Triaxial	6×10^{-6} $3.6\mu\text{m}/\text{mn}$ $H = 50 \text{ mm}$
Chiarelli (2000), Chiarelli et al. (2003)	EST 02277	469	100	35	11 – 13.5* <i>Est. 14.6 – 18</i>	4 – 7	85 – 100	Triaxial	6×10^{-6} $3.6\mu\text{m}/\text{mn}$ $H = 50 \text{ mm}$
Chiarelli (2000), Chiarelli et al. (2003)	EST 02354	482	100	35	11.8 – 13.8* <i>Est. 15.7 – 18.4</i>	4 – 7	90 – 100	Triaxial	6×10^{-6} $3.6\mu\text{m}/\text{mn}$ $H = 50 \text{ mm}$
Zhang & Rothfuchs (2004)	EST 05677-02	487	80	40	16.1	7.1	99	UCS	6.5×10^{-6} $3.1\mu\text{m}/\text{mn}$ $H = 40 \text{ mm}$
Zhang & Rothfuchs (2004)	EST 05677-04	487	80	40	16.1	2.8	39	UCS	6.5×10^{-6} $3.1\mu\text{m}/\text{mn}$ $H = 40 \text{ mm}$
Zhang & Rothfuchs (2004)	EST 05677-01	487	98	50	16.1	7.1	99	Undrained triaxial multistage	6.5×10^{-6} $3.8\mu\text{m}/\text{mn}$ $H = 49 \text{ mm}$
Pham et al. (2007)	EST 205D	451	72	36	10 – 14	1.65 – 5.24	Various S_r	UCS	Not given
(2014a)	EST 30446	521.5	20	20	11.8	6.2	100	Triaxial	10^{-7} s^{-1} $0.12\mu\text{m}/\text{mn}$ $H = 10 \text{ mm}$

* porosity value obtained by Chiarelli et al. (2003) from mercury intrusion porosimetry tests. Estimated total porosity values are given in italics based on our observation that 25% of the total porosity was not intruded at 200 MPa in the tests that we performed on COx specimens at 490 m.

Table 3

Table 3. Experimental programme.

Test	Specimen	Ref. Core	Programme	Permeability test
T1	S1	EST45414	Shear under $\sigma' = 8\text{MPa}$ at 25°C [B-C]	-
T2	S2	EST30734	Isotropic unloading to $\sigma' = 4\text{MPa}$ (swelling) [B-C], shear at 25°C [C-D]	-
T3	S3	EST28514	Isotropic unloading to $\sigma' = 4\text{MPa}$ (swelling) [B-C], shear at 25°C [C-D]	-
T4	S4	EST28518	Drained isotropic compression up to $\sigma' = 16\text{MPa}$ [B-C], shear at 25°C [C-D]	-
T5	S1	EST45414	Drained heating up to 80°C [B-C], shear under $\sigma' = 8\text{MPa}$ at 80°C [C-D]	-
T6	S5	EST45407	Isotropic unloading to $\sigma' = 4\text{MPa}$ [B-C], drained heating up to 80°C [B-C], shear at 80°C [C-D]	[B], [C], [D]

Table 4

Table 4. Evolution of the elastic parameters.

Test	Ref. Core	Porosity (%)	σ' (MPa)	Temperature (°C)	q_{max} (MPa)	E_1 (GPa)	ν_{12}
T1	EST45414	13.0	8	25	23.1	3.2	0.30
T2	EST30734	16.5	4	25	10.5	1.5	0.10
T3	EST28514	17.6	4	25	10.3	1.3	0.10
T4	EST28518	17.8	16	25	24.6	5.5	0.34
T5	EST45414	13.0	8	80	20.0	3.4	0.26
T6	EST45407	13.5	4	80	16.1	1.4	0.10

Table 5

Table 5. Thermal contraction coefficients.

Specimen	Ref. Core	σ' (MPa)	Depth (m)	Porosity (%)	$C_{T//}$ ($\times 10^{-5} \text{ }^\circ\text{C}^{-1}$)	$C_{T\perp}$ ($\times 10^{-5} \text{ }^\circ\text{C}^{-1}$)
S5	EST45414	8	491	13.0	1.06	1.15
S6	EST45407	4	491	13.5	0.77	0.96
Mohajerani et al. (2014)	EST25820	8	480	17.9	3.15	6.50

Table 6Table 6. Effect of swelling and temperature on the CO_x claystone permeability (T6, porosity 13.5 %).

State	Test	Ref. Core	$k_{r \text{ inflow}} \text{ (m}^2\text{)}$	$k_{r \text{ outflow}} \text{ (m}^2\text{)}$
After resaturation, 25°C, [B]	T6	EST45407	1.1×10^{-20}	0.9×10^{-20}
After swelling, 25°C, [C]	T6	EST45407	1.6×10^{-20}	1.4×10^{-20}
After heating, 80°C, [D]	T6	EST45407	2.9×10^{-20}	1.8×10^{-20}

Figure 1

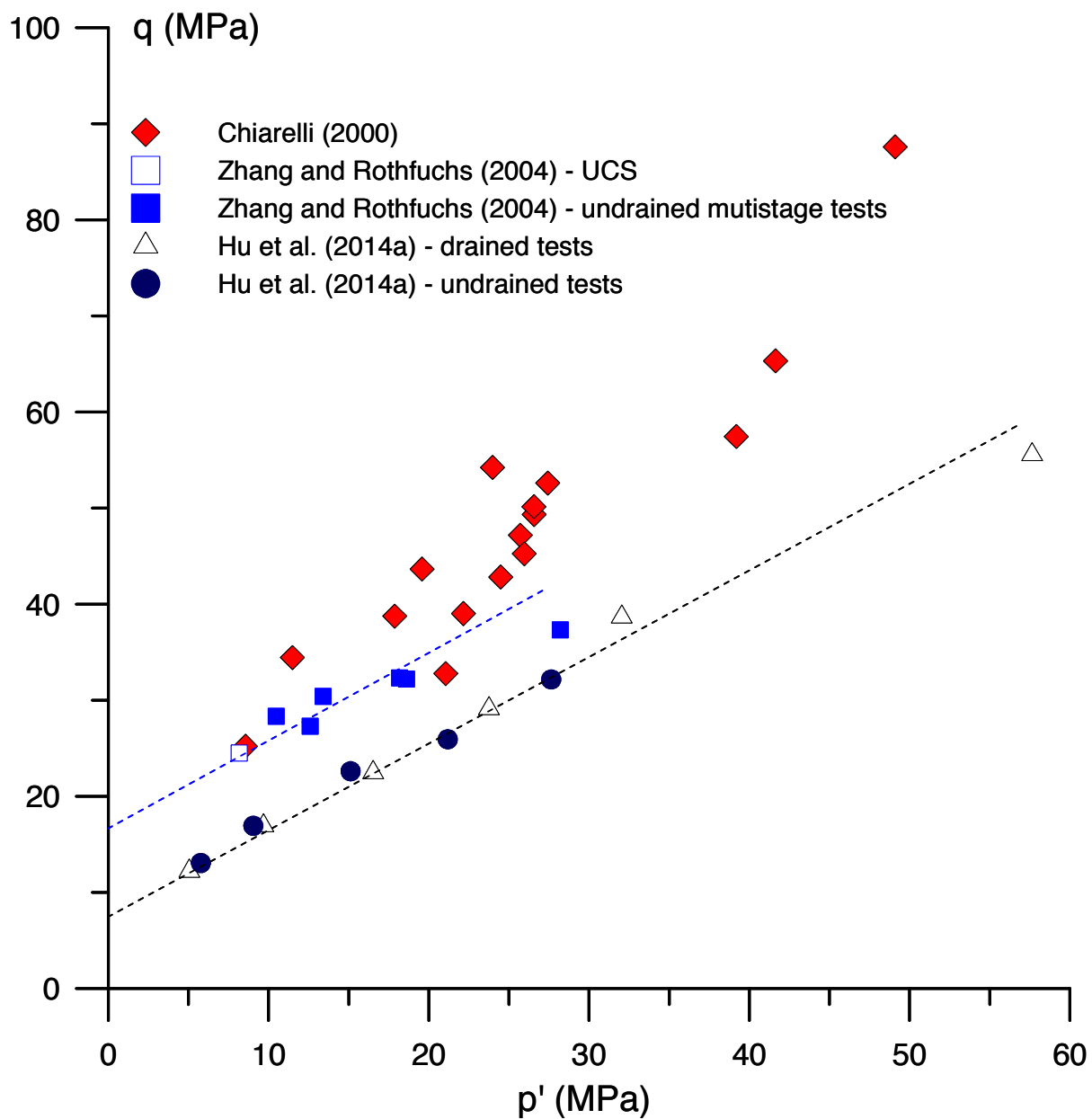


Fig. 1. Published shear strength data of the COx claystone.

Figure 2

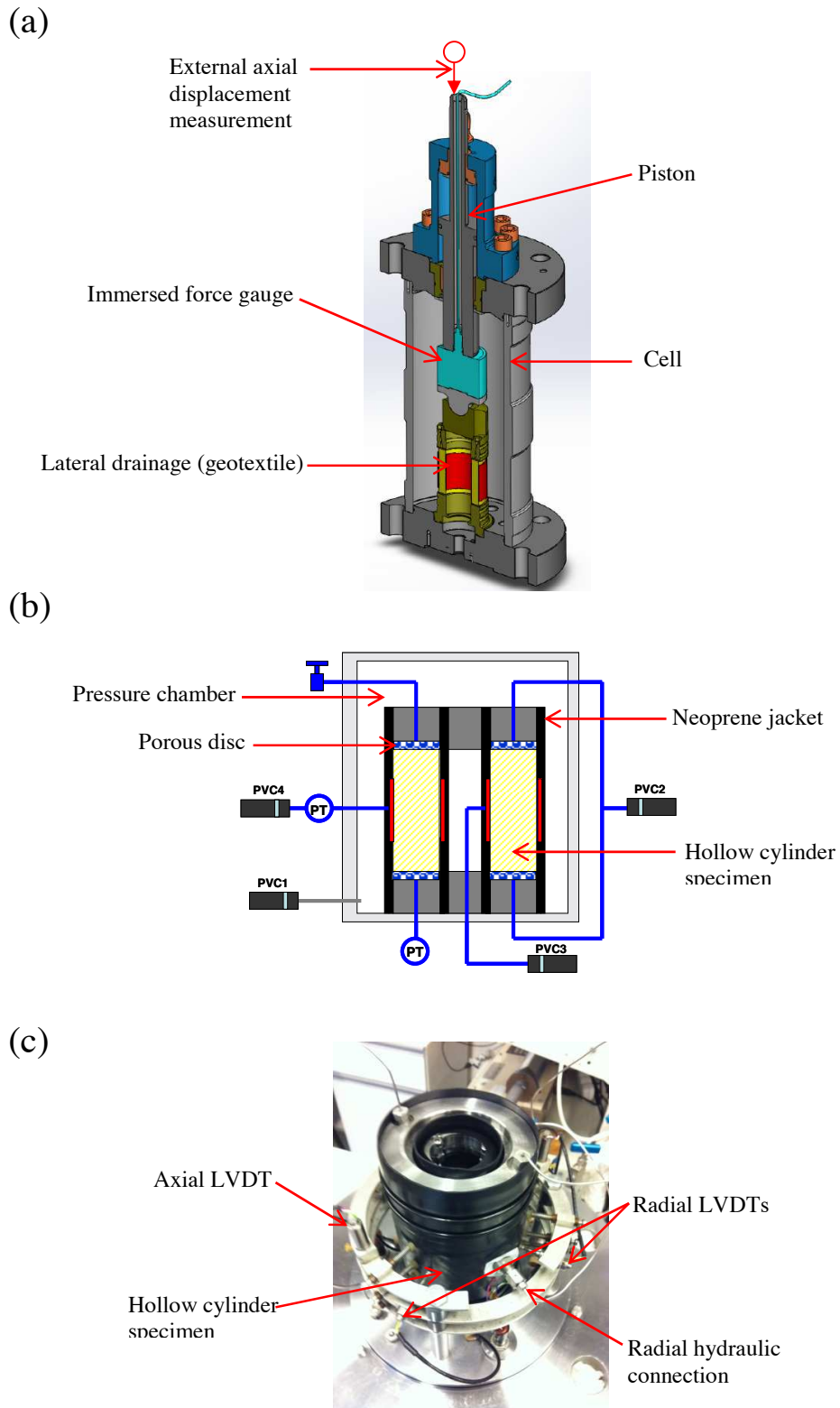


Fig. 2. (a): Hollow cylinder triaxial cell, (b): Scheme of the hydraulic connections, (c): Local strain measurement system.

Figure 3

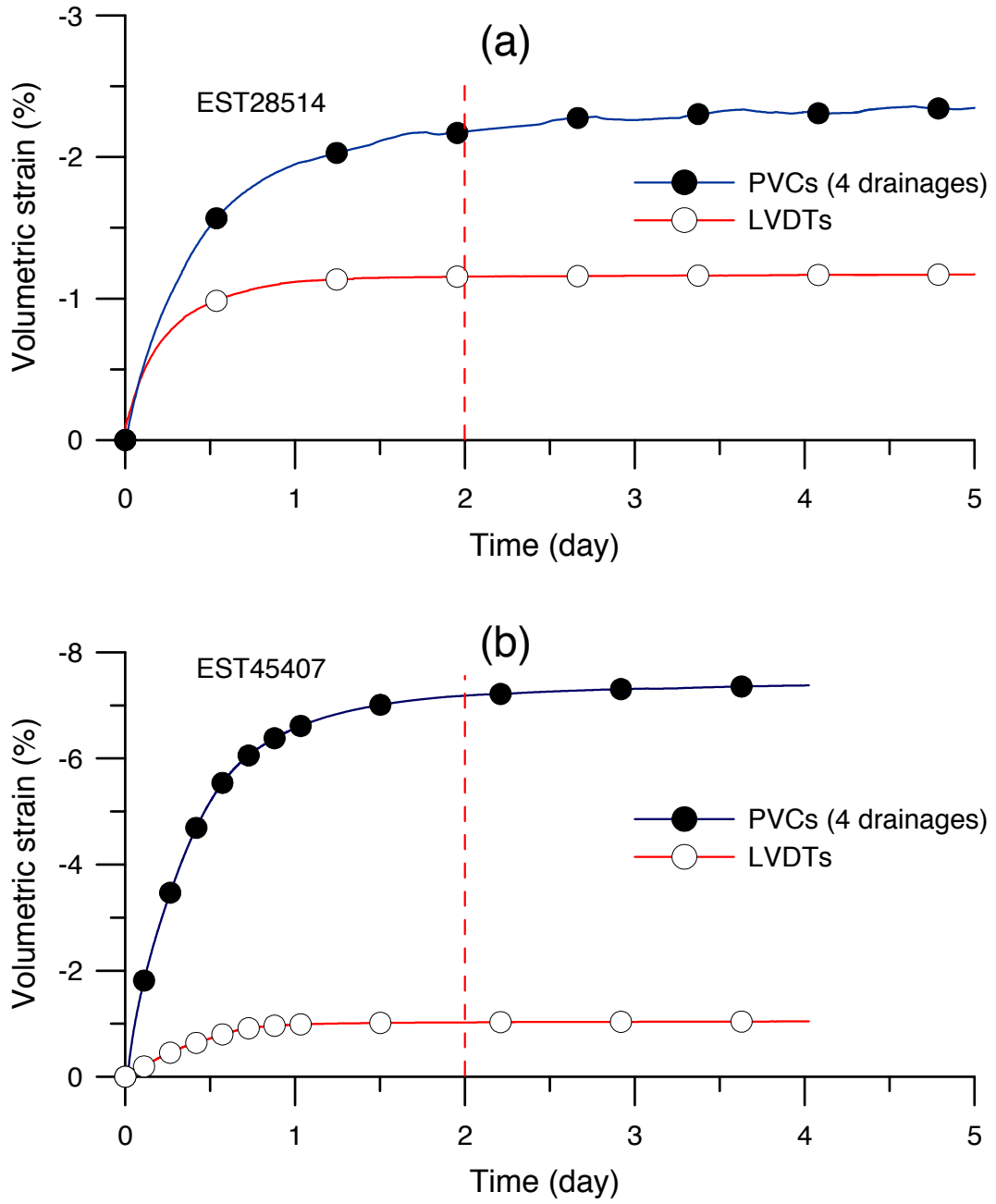


Fig. 3. Volume changes and water exchanges during resaturation phase; (a) test T3, (b) test T6.

Figure 4

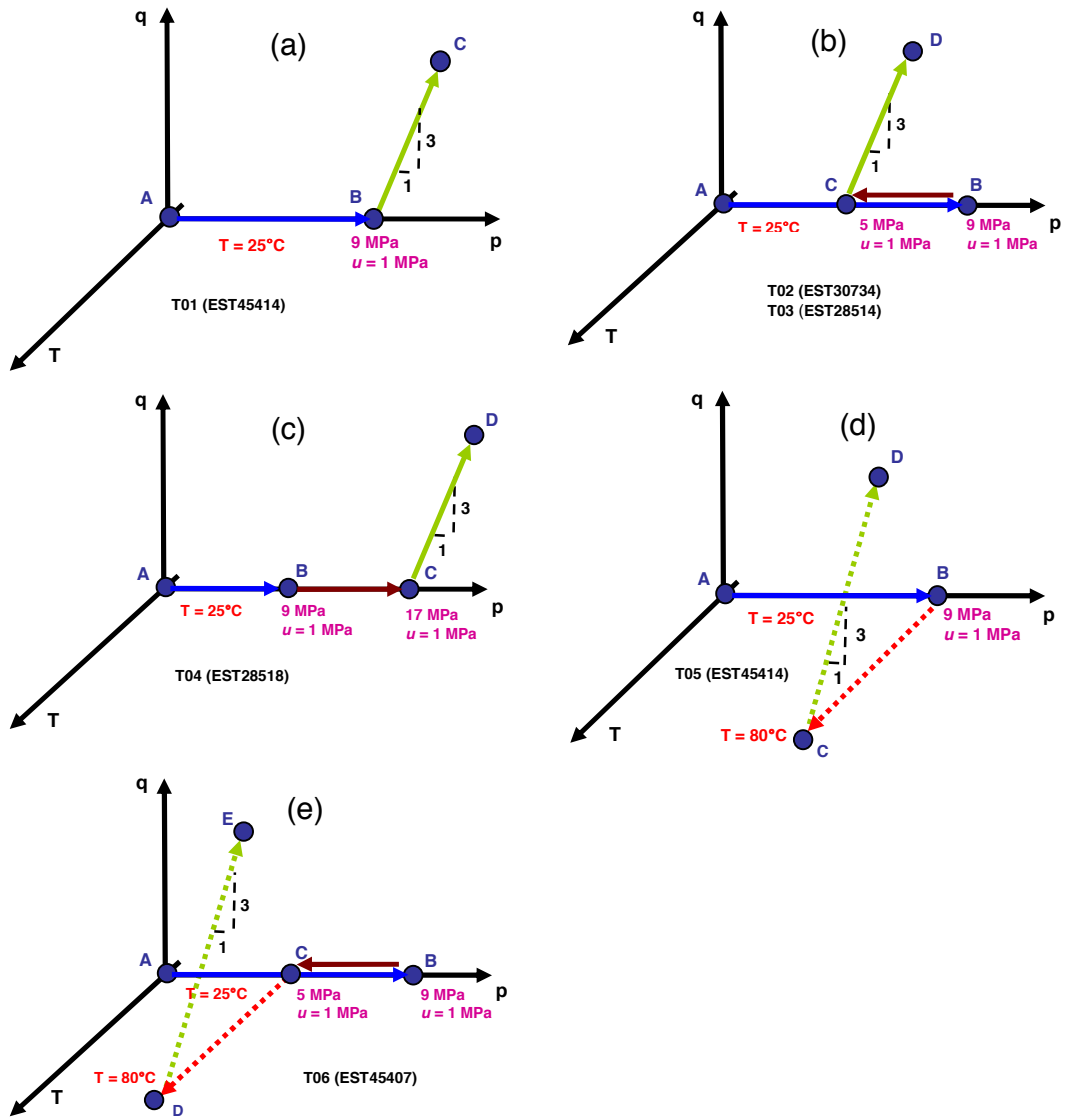


Fig. 4. Thermo-hydro-mechanical paths followed during the tests carried out.

Figure 5

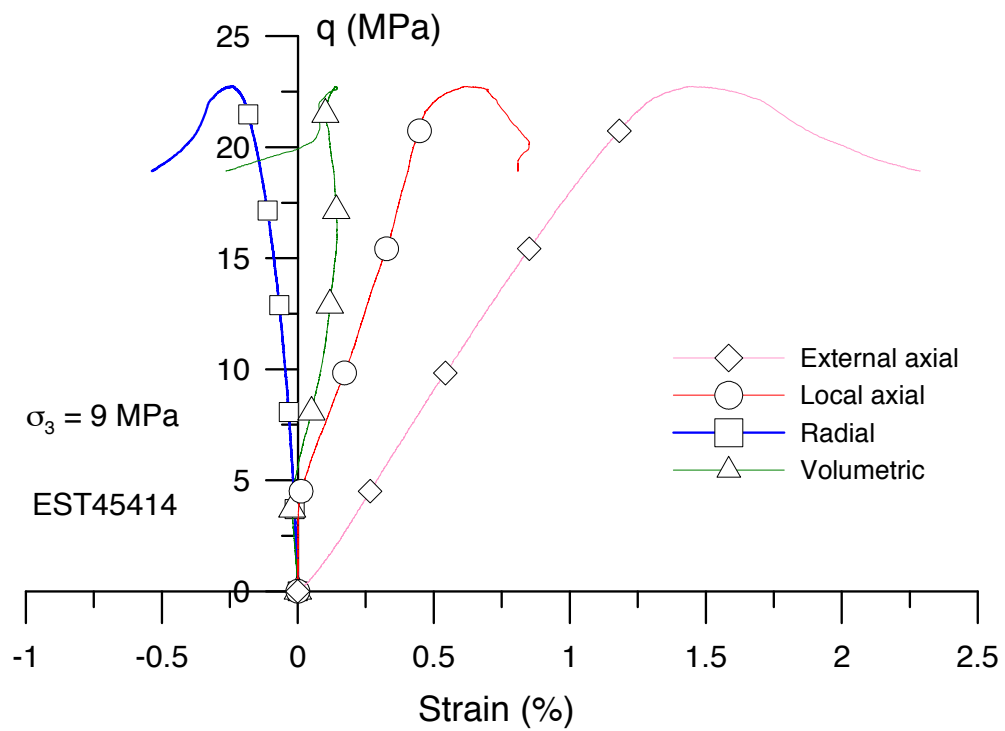


Fig. 5. Drained shear test under in-situ effective stresses at 25°C, test T1.

Figure 6



Fig. 6. COx claystone at the end of the test T1.

Figure 7

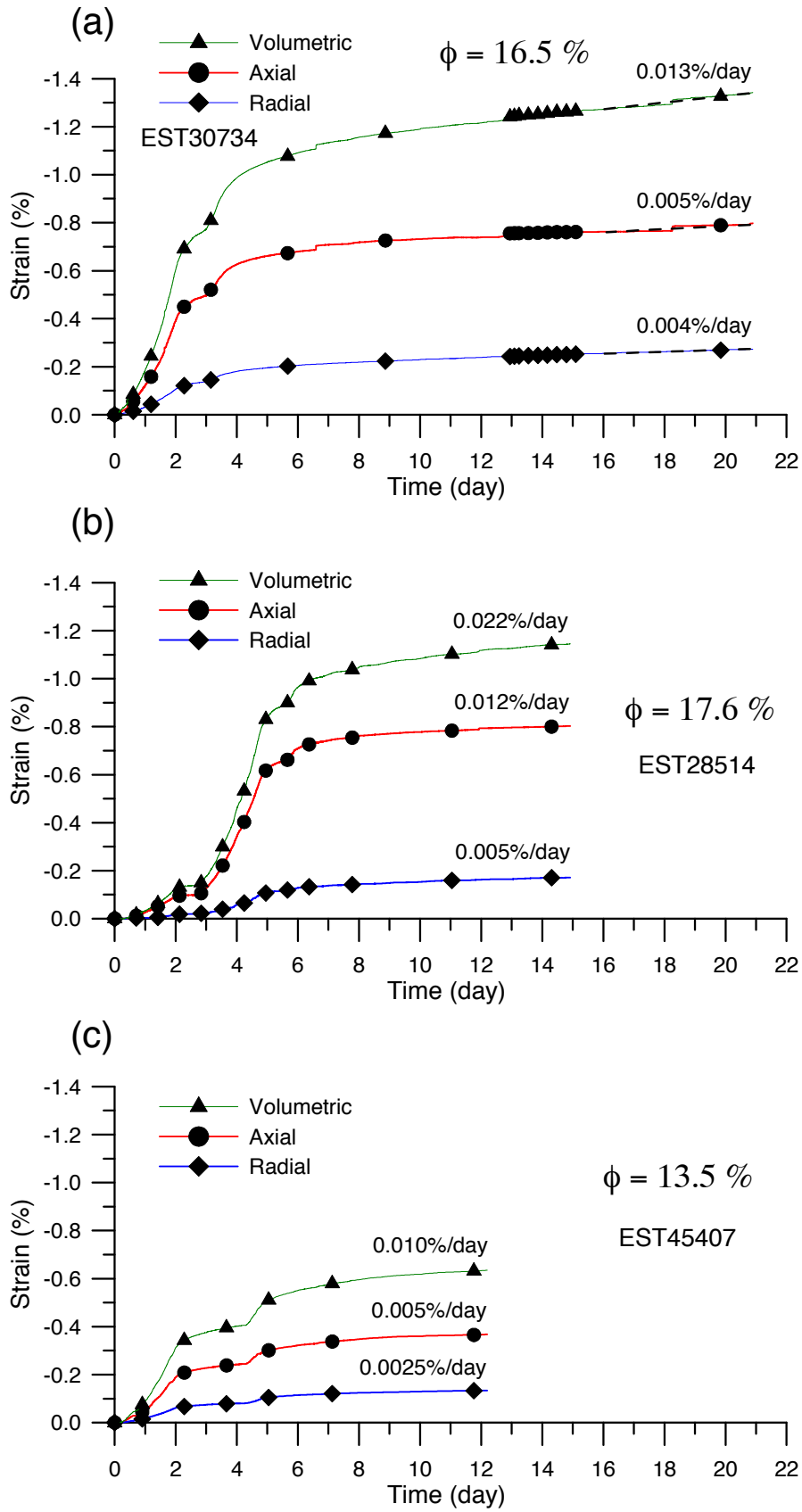


Fig. 7. Drained isotropic unloading phase, (a): T2, (b): T3, (c): T6.

Figure 8

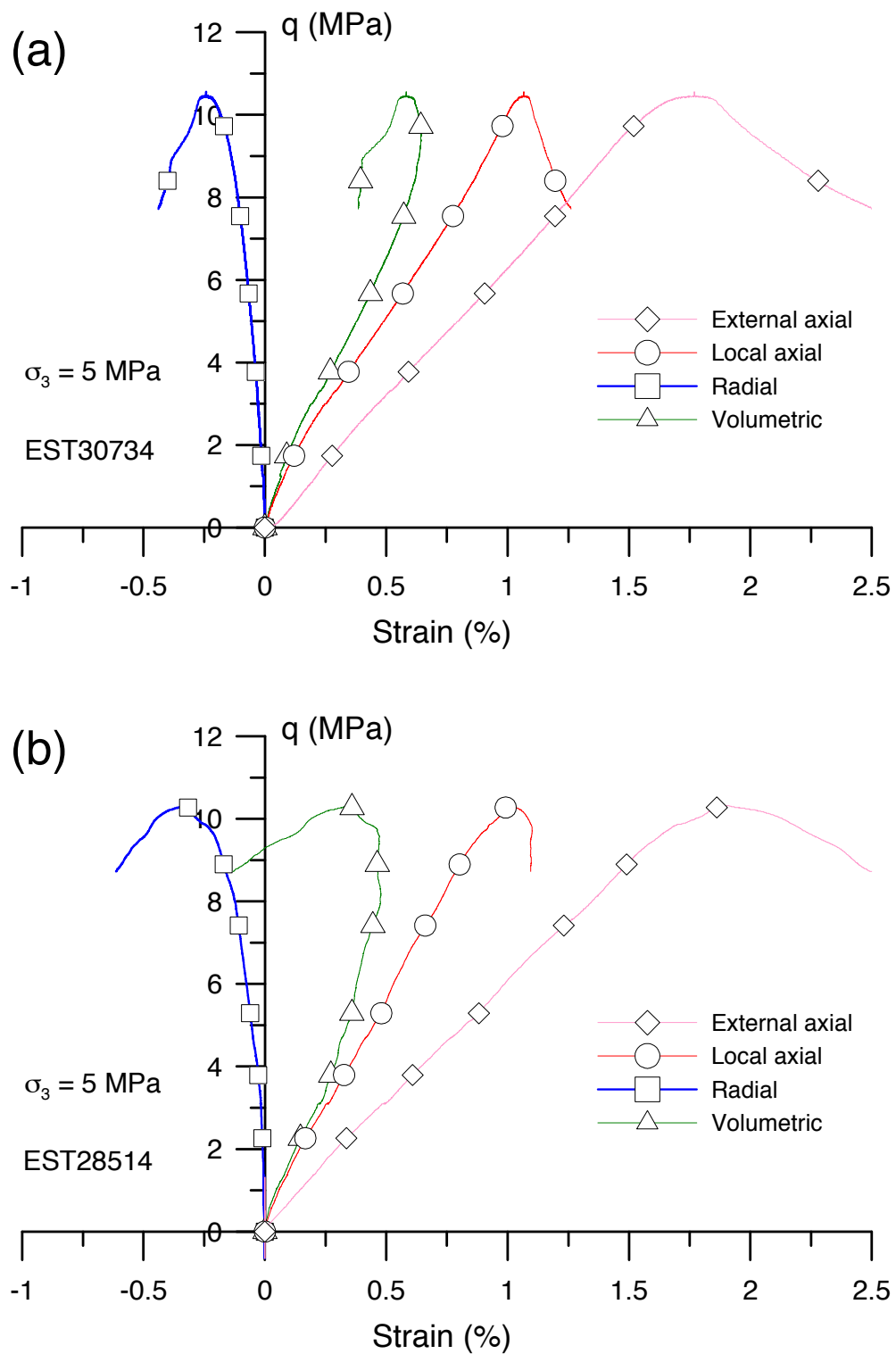


Fig. 8. Drained shear test under half in-situ effective stresses at 25°C, (a): test T2, (b): test T3.

Figure 9

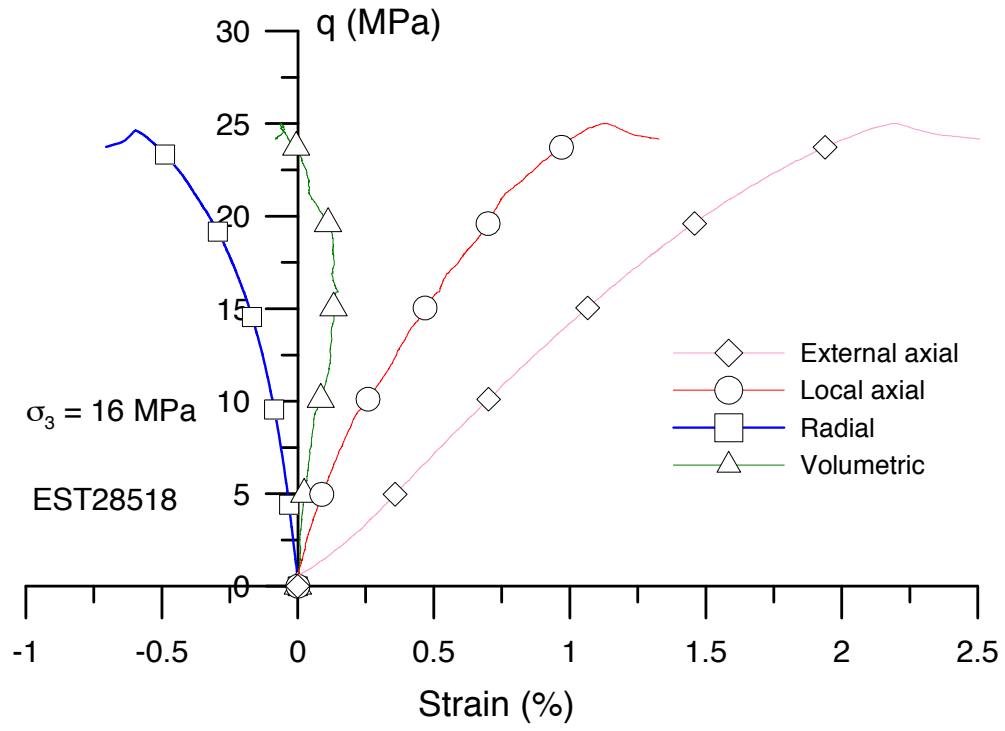


Fig. 9. Drained shear test under twice in-situ effective stresses at 25°C, test T4.

Figure 10

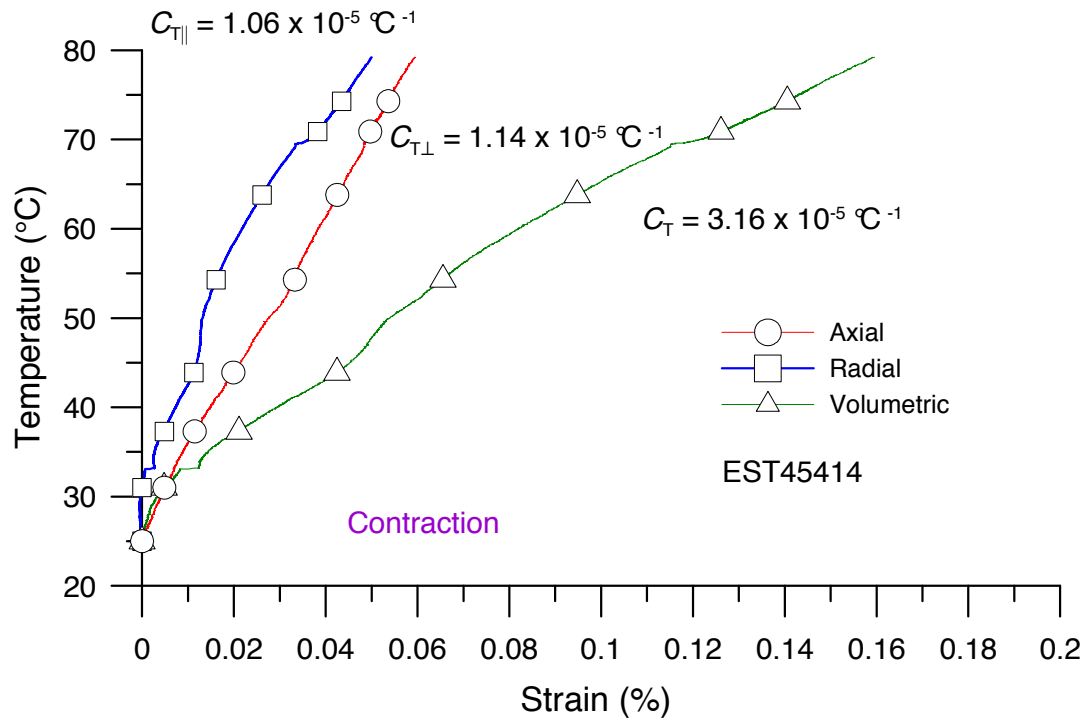


Fig. 10. Axial, radial and volumetric strains measured during a drained heating test (0.5°C/h) under in-situ effective stresses, test T5.

Figure 11

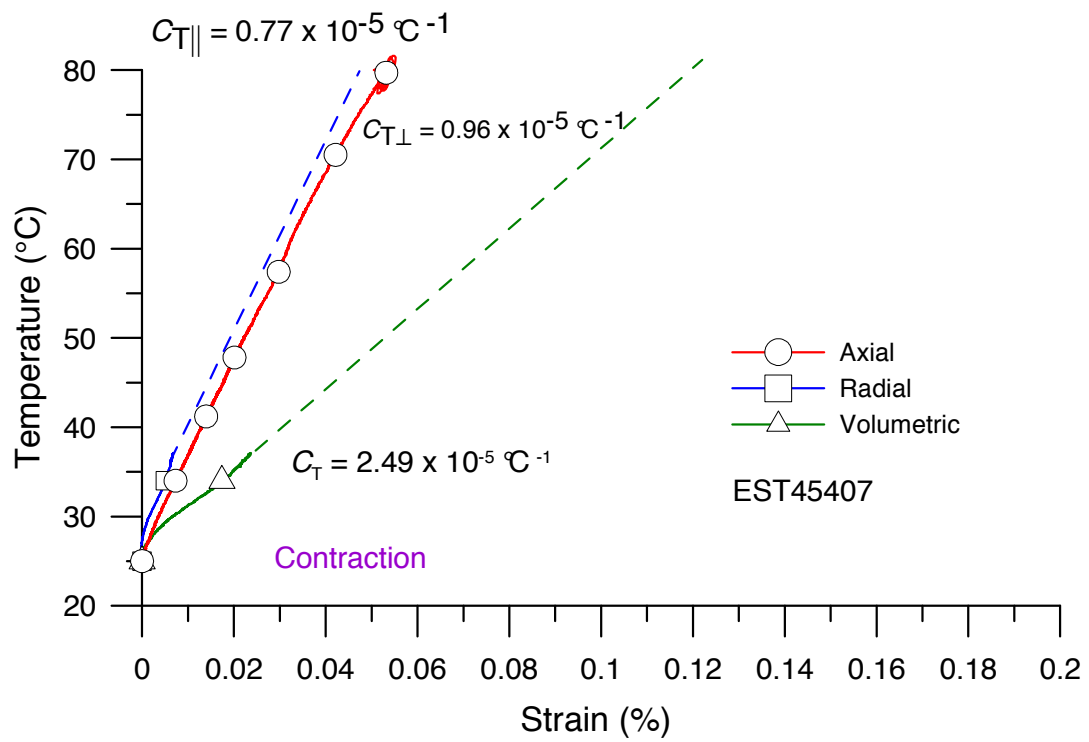


Fig. 11. Axial, radial and volumetric strains measured during a drained heating under half in-situ effective stresses, test T6.

Figure 12

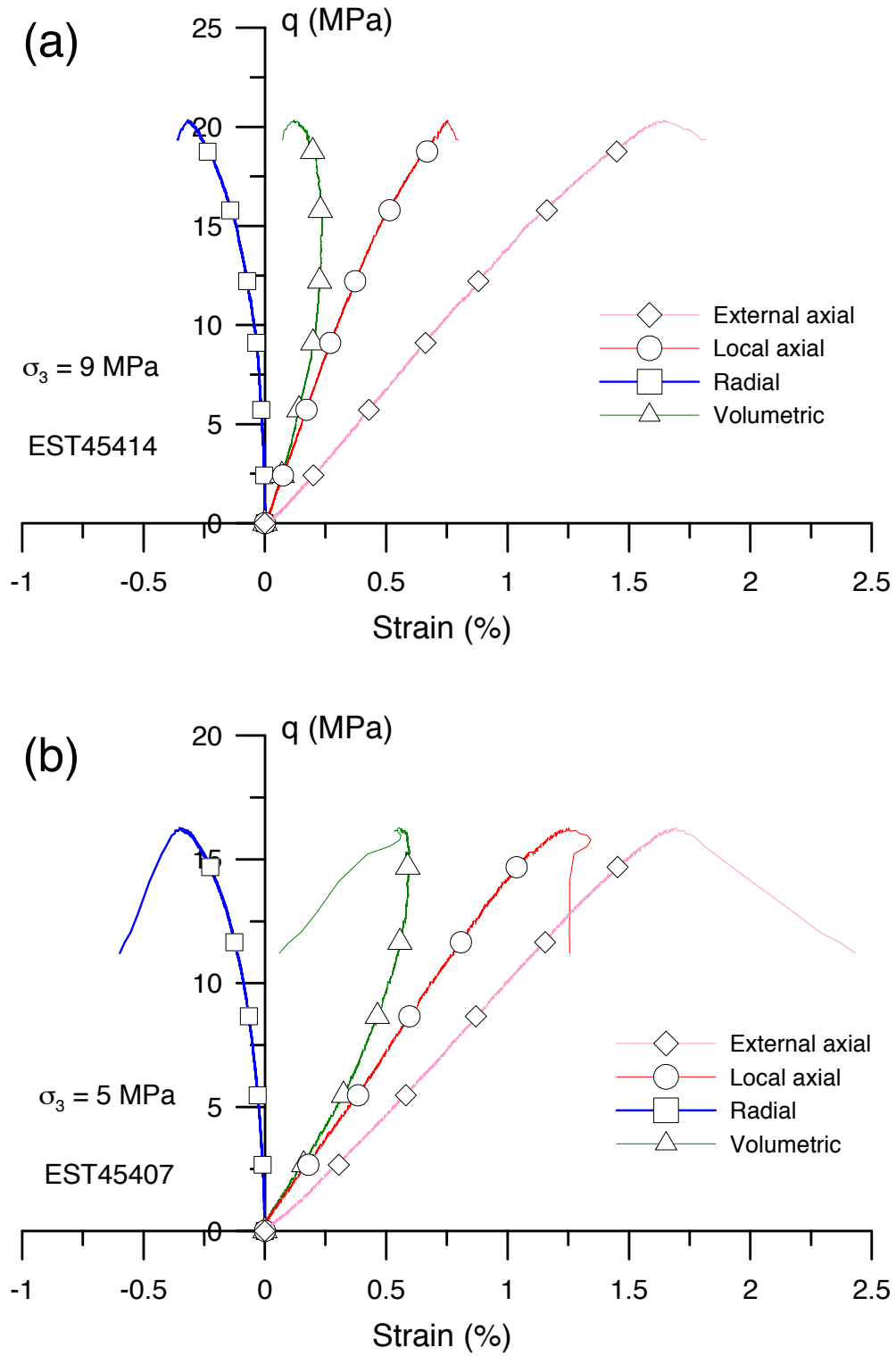


Fig. 12. Drained shear test at 80°C, (a): test T5, (b): test T6.

Figure 13

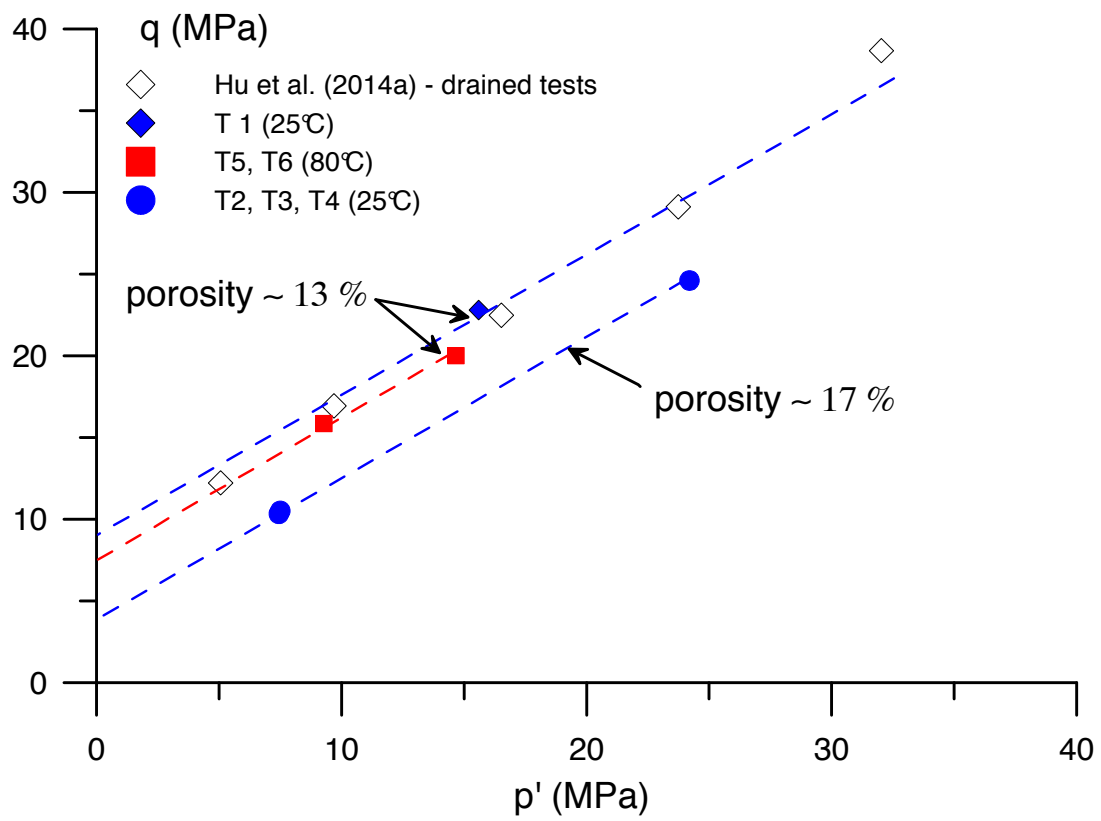


Fig. 13. Shear strength of all tests carried out in the plan q-p'.

Figure 14

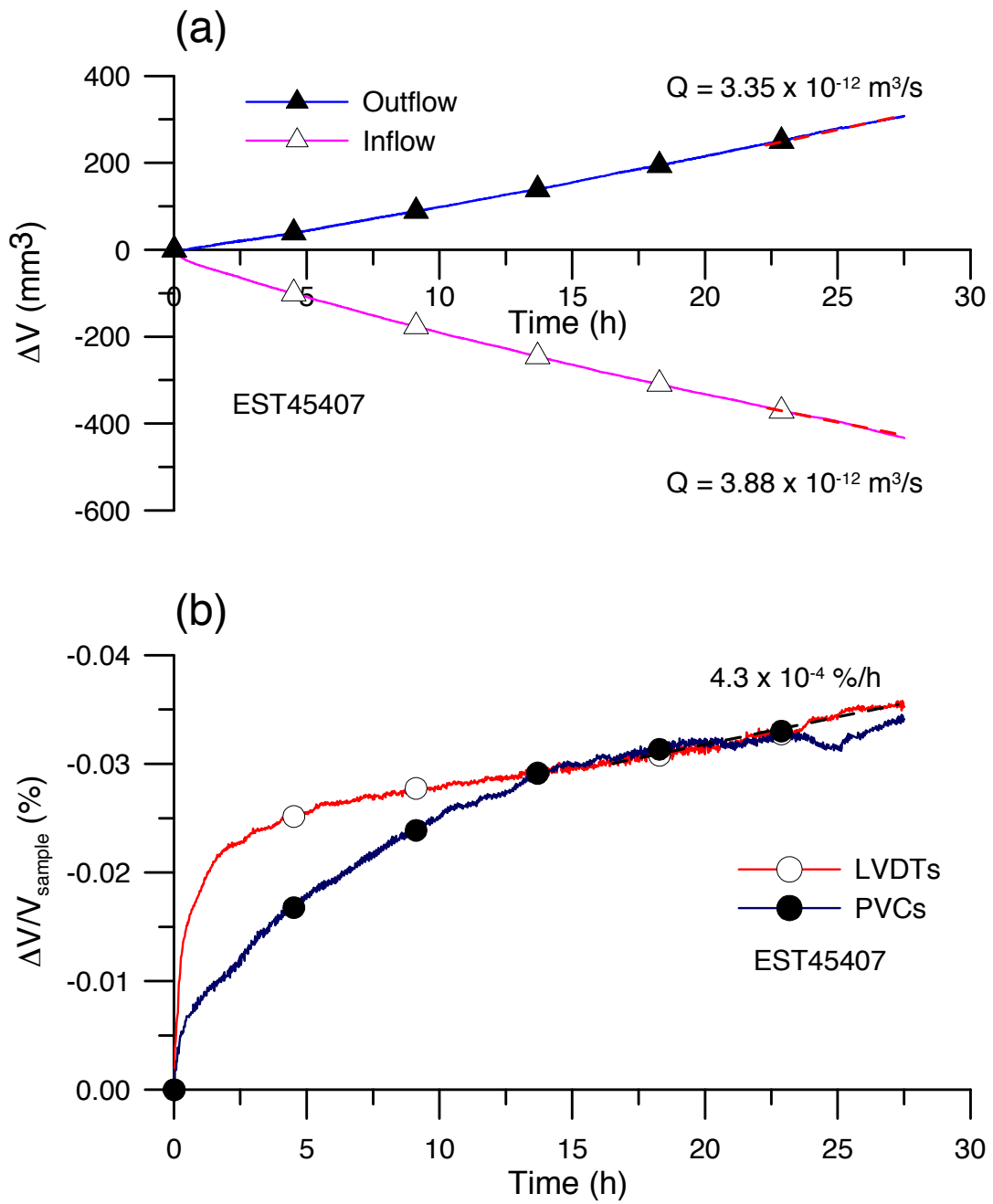


Fig. 14. Radial permeability test at point B, after resaturation T6, (a): inflow and outflow, (b): volume change.

Figure 15

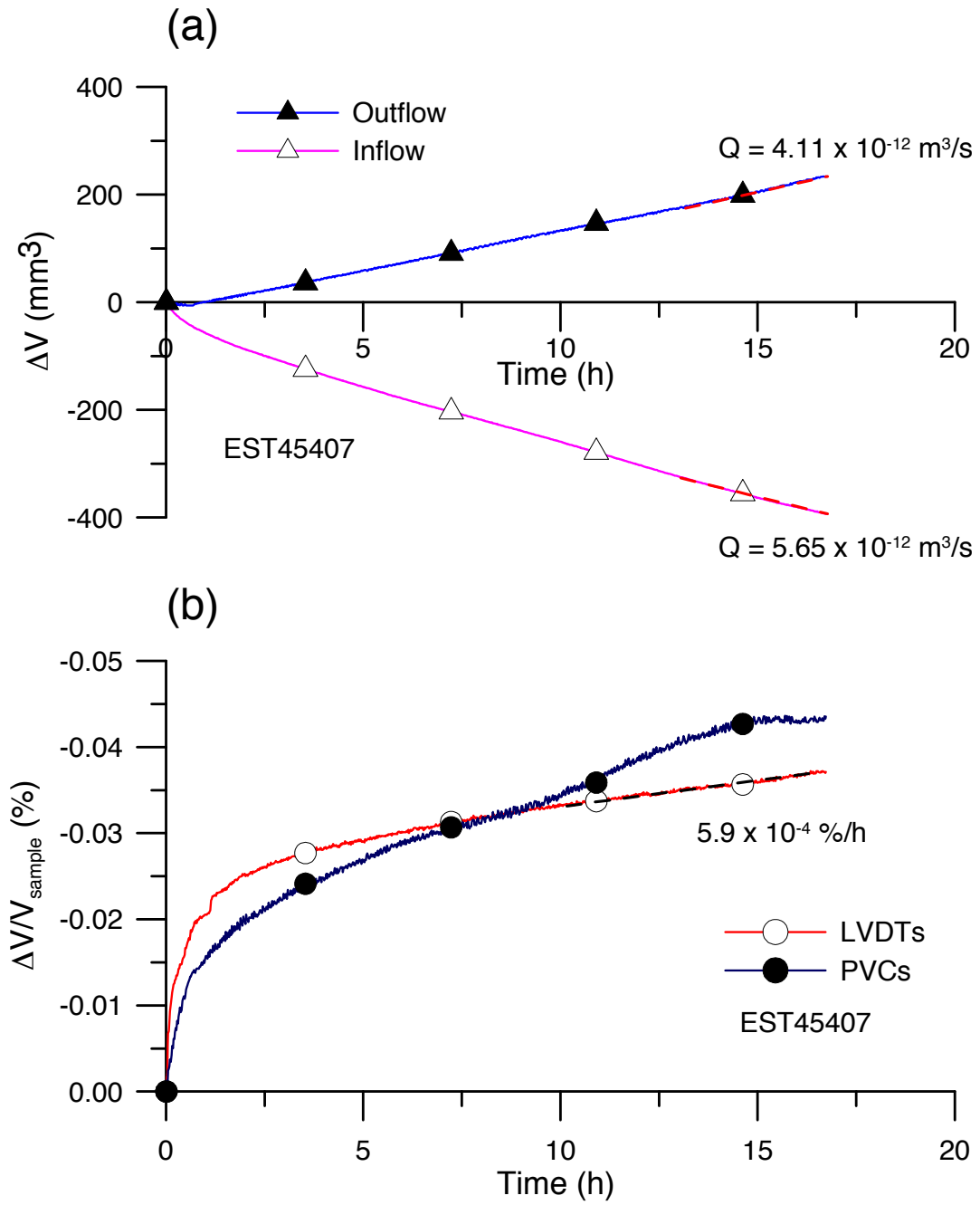


Fig. 15. Radial permeability test at point C, after swelling T6, (a): inflow and outflow, (b): volume change.

Figure 16

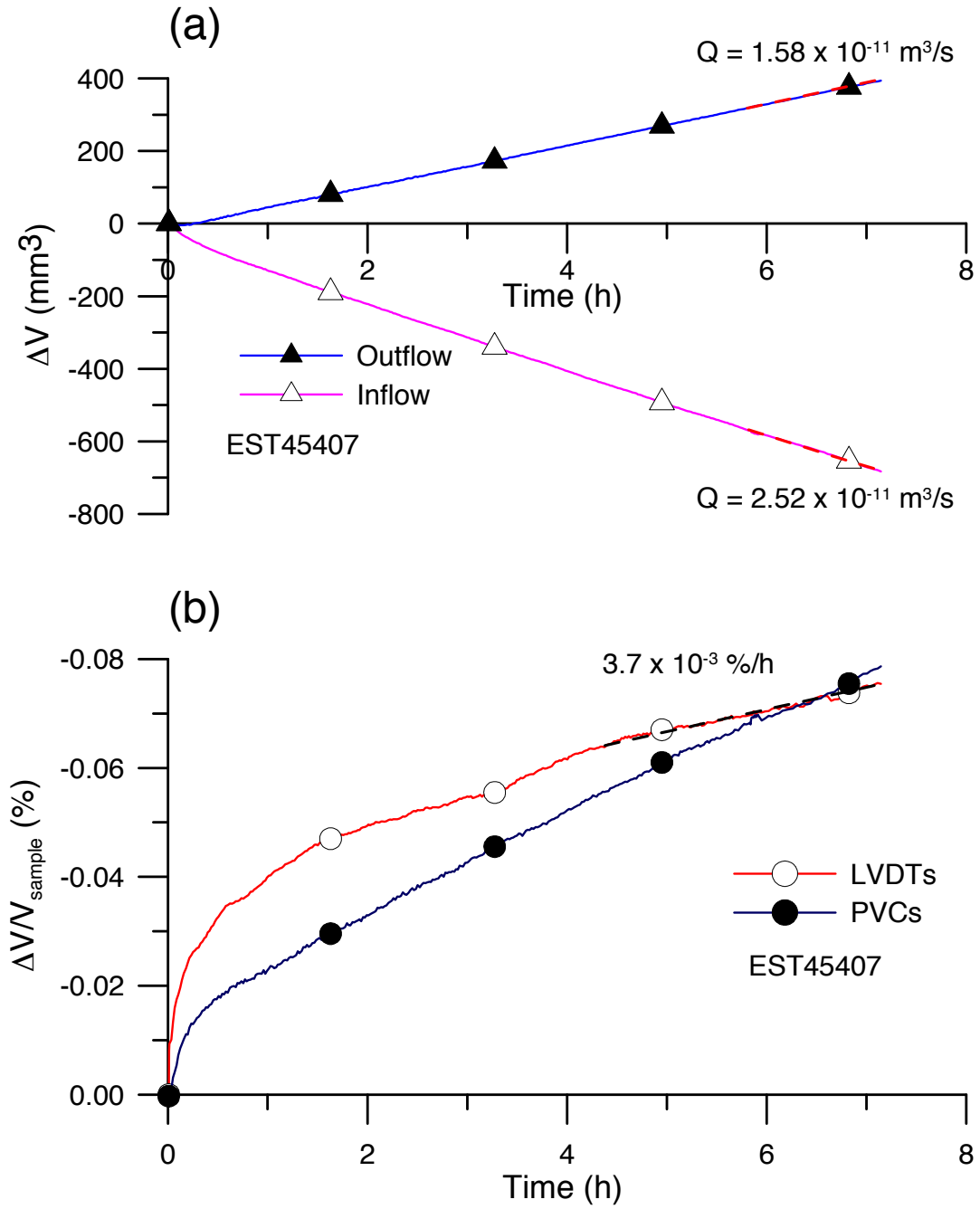


Fig. 16. Radial permeability test at point D, after heating T6, (a): inflow and outflow, (b): volume change.

Figure 17

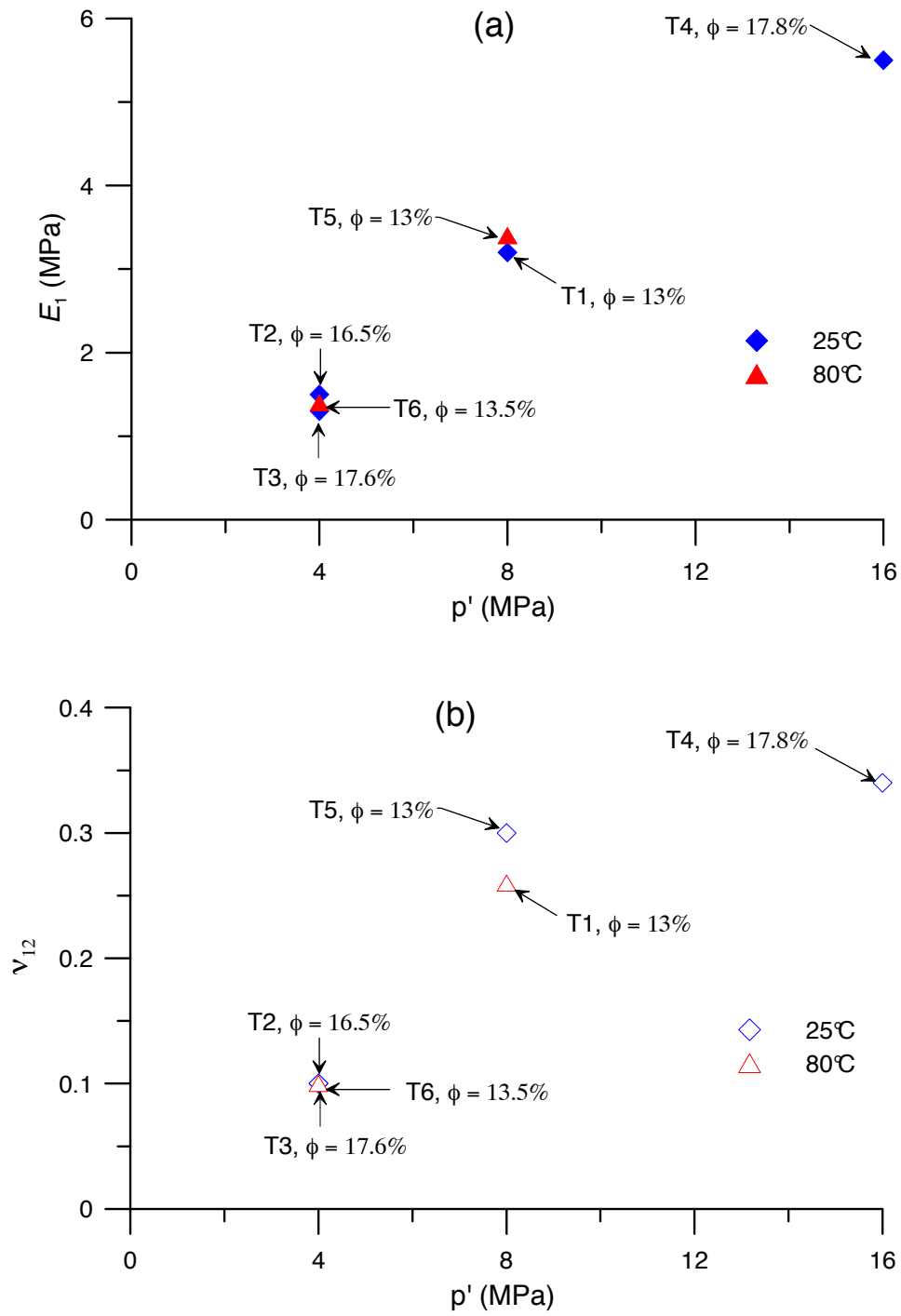


Fig. 17. Elastic parameters, (a): Young's modulus, (b): Poisson coefficient.